Fall 2020

Additive manufacturing of linear shaped charges to address run up and run down phenomena

Jason Ho

Department:

ADDITIVE MANUFACTURING OF LINEAR SHAPED CHARGES TO ADDRESS RUN UP AND RUN DOWN PHENOMENA

by

JASON HO

A THESIS

Presented to the Faculty of the Graduate School of the

MISSOURI UNIVERSITY OF SCIENCE AND TECHNOLOGY

In Partial Fulfillment of the Requirements for the Degree

MASTER OF SCIENCE IN EXPLOSIVES ENGINEERING

2020

Approved by:

Dr. Catherine Johnson, Advisor
Dr. Paul Worsey
Dr. Phillip Mulligan

ABSTRACT

A shaped charge is an explosive device used to focus detonation energy in a desired direction. Additive Manufacturing (AM) can allow greater design freedom and geometric complexity for the liner portion of the shaped charge.

In this work, the following hypotheses were tested: 1) Adjusting the initial apex angle of a linear shaped charge liner reduces the amount of run up that occurs, and 2) implementing a backstop at the end of a linear shaped charge liner reduces the amount of run down that occurs.

Linear shaped charge liners with a continuously changing apex angle were created with additive manufacturing. Three separate sets of liner bases were created: two sets had initial apex angles of 55 and 70 degrees respectively, and the third set served as a standard with an initial apex angle of 85 degrees.

Linear shaped charge liners with backstops were also created with additive manufacturing. Backstops of 1x, 2x and 3x the thickness of the liner were implemented at the end of the liner top to test effectiveness in reducing run down.

The results from testing hypothesis 1 indicated that changing the apex angle yielded little reduction in the run up area, however, the overall penetration depth was deeper with the more acute initial apex angle. The results from testing hypothesis 2 indicated that the backstop greatly reduced the run down area. A third experimental test series was developed to test the combination of the apex angle change and the backstop and showed high repeatability. The use of additive manufacturing to create linear shaped charge liners was successful.

ACKNOWLEDGMENTS

I would like to thank my advisor, Dr. Catherine Johnson, for her guidance, encouragement, and extreme patience during the completion of this thesis, and my committee members, Dr. Paul Worsey and Dr. Philip Mulligan, for their valuable input and mentoring.

On a personal note, I would like to thank all of my family for their love and continuous support during this time, especially my wife, Jill, who has been a pillar of support and love.

Finally, I would like to thank the following people: Cody for printing all of the liners used for testing, Jeff and all his expertise in the workshop to help make my testing results useable, Marty for all his help with my testing and always being there to offer a different point of view, Barbara for all her help with editing and proofreading, and all of Dr. Johnson's graduate students for being there to support with testing and prep work and to bounce ideas off of.

TABLE OF CONTENTS

LIST OF ILLUSTRATIONS

Page

LIST OF TABLES

Page

NOMENCLATURE

Symbol	Description
LSC	Linear shaped charge
SLM	Selective laser melting
PETN	Pentaerythritol tetranitrate
SCAP	Shaped Charge Analysis Program
CTH	Modeling software
g	Grams
cc	Cubic centimeter
cm^3	Cubic centimeters
°C	Celsius
cm	Centimeter
in	Inches
ft	Feet
°	Degree
CAD	Computer aided design
ISO	International Organization for Standardization
ASTM	American Society for Testing and Materials
CO_2	Carbon dioxide
IR	Infrared
SHS	Selective heat sintering
SLS	Selective laser sintering

DMLS	Direct metal laser sintering
EBM	Electron beam melting
MJF	Multi jet fusion
C4	Composition C-4

1. INTRODUCTION

A shaped charge can be defined as an explosive charge that contains a hollow cavity, which allows the charge to focus its energy into a specific area [1]. By focusing and directing the energy towards a specific area or object, such as a metal plate or a block of concrete, the shaped charge can penetrate hard surfaces and objects in microseconds what might take drilling or sawing methods hours or days to penetrate. If the hollow cavity is lined with a thin layer of metal, the liner may form a jet when the explosive is initiated that increases the penetration effect of the shaped charge. Shaped charges are used in various disciplines, from demolition to aerospace engineering, oil well drilling to military applications.

Like its name implies, LSCs are straight-edged charges that make up a small, niche branch of the shaped charge family. LSCs come in different sizes, typically referred to as grains, depending on the task at hand. They are often used to quickly, remotely, and efficiently cut through objects that may otherwise take considerable time and effort to do so. While they are the preferred tools of choice to use in their industry, predominantly demolition, they are not without shortcomings.

Two shortcomings of using LSCs are the run up and run down that routinely occur. Run up refers to the area in the initial stages of the target where the depth of penetration is constantly increasing until it reaches a constant depth of cut and stabilizes. In a similar vein, run down refers to the area in the latter stages of the target where the depth of penetration decreases from its stable cut due to energy loss out the end of the LSC. Figure 1.1 displays the areas referred to as the run up and run down zones.

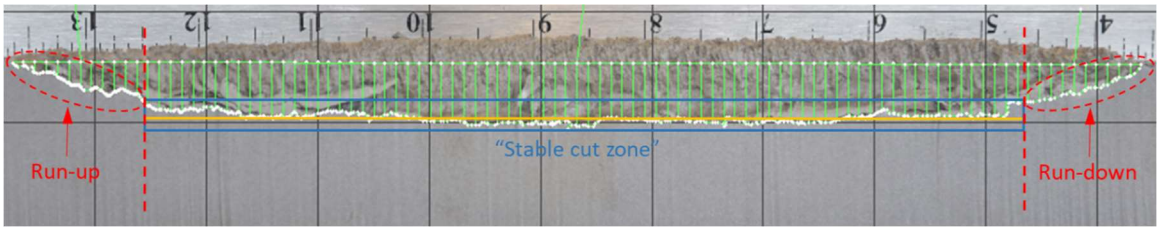

Figure 1.1 Image of a steel target cut in half to display penetration achieved with a LSC. The cut made by the LSC is traced by the white line. The run up and run down areas are labeled in red.

Current procedures utilizing LSCs consist of allowing parts of the LSC extend beyond the target cut area, such that both ends of the LSC hang over the edge of the target. Not only is this a waste of liner and explosive materials, but fragments from the LSC or even the blade itself can be dangerous during a sensitive and expensive operation, such as cutting off unfired detonating cord or shot wire.

Current conventional manufacturing of LSCs consists of creating the liner as one solid, metallic, circular tube and then loading the explosives into the liners. Once filled with explosives, the LSC is run through a forming die until the desired 'V' shape is formed [2]. These long sheaths of LSCs are then cut into standard lengths to distribute commercially. Additive manufacturing can allow for geometric complexity not possible in conventional manufacturing techniques.

This thesis investigates the use of SLM to additively manufacture LSC liners that reduce the run up and run down effect when using LSCs. By decreasing the initial apex angle, a deeper initial penetration might be produced that would reduce the distance to maximum penetration, thus reducing the amount of run up that occurs. The addition of a

backstop to contain the energy at the exit could potentially reduce the amount of run down that occurs.

The hypothesis to be tested is as follows:

1. The amount of run up and run down that occurs when using LSCs can be diminished through customization of the LSC's liner.

a) The run up can be reduced by implementing a more acute apex angle in the LSC at the initiation front.

b) The run down can be reduced by implementing a backstop to force the energy in a downward direction.

Additive manufacturing will be utilized to create liners to test these two aspects of liner geometry and their effects on run up and run down. A conclusion will be made based on the analysis of the results to determine if there is strong evidence to support or reject the null hypothesis.

The following work will include background information on LSCs and the additive manufacturing processes used to create the custom LSC liners in Section 2. The methodology in designing, manufacturing, and testing these additively manufactured LSC liners will be explained in detail in Section 3. The results of the testing will then be provided along with analysis of said results will be described in Section 4.

2. LITERATURE REVIEW

A majority of shaped charge history and research revolves around the conical shaped charge and its militaristic applications, due to its propensity for penetrating through heavy armor. However, a need to penetrate thick metal outside of the war zone lead to the development of the linear shaped charge and its commercial uses [3]. A full literature review of the following will be discussed throughout this section: history of shaped charges, theory of shaped charges, and additive manufacturing methods.

2.1. BRIEF HISTORY OF SHAPED CHARGES

Shaped charges come in all manner of sizes and shapes, including but not limited to conical shaped charges, hemispherical shaped charges, and linear shaped charges. Charles E. Munroe is credited with the rediscovery of the shaped charge effect [4]. Although there were earlier instances of void-shaped hollows in explosives and the increased power provided due to these voids, the shaped charge effect is now known as the Munroe Effect [5, 6]. Munroe rediscovered this in 1888 while working as a civilian chemist at the Naval Torpedo Station. Munroe observed that when a hollow cavity is present in an explosive charge, opposite the initiation end, the resulting crater in the target has increased depth and penetration compared to an explosive charge sans hollow cavity [3].

In 1957, Ensign-Bickford proceeded to design linear shaped charges intending to take advantage of the Munroe Effect. Their initial design consisted of lead tubes fashioned in a “D” shape and loaded with PETN, which was able to cut through $1/8^{th}$ inch

of 6061 aluminum with a 30 grain per foot charge. This design was later developed into a "U" shaped charge, as shown in Figure 2.1, that could also cut through 1/8th inch of aluminum while using less explosive (20 grain per foot less) and producing less damage to a second target plate positioned directly above the explosive charge [3].

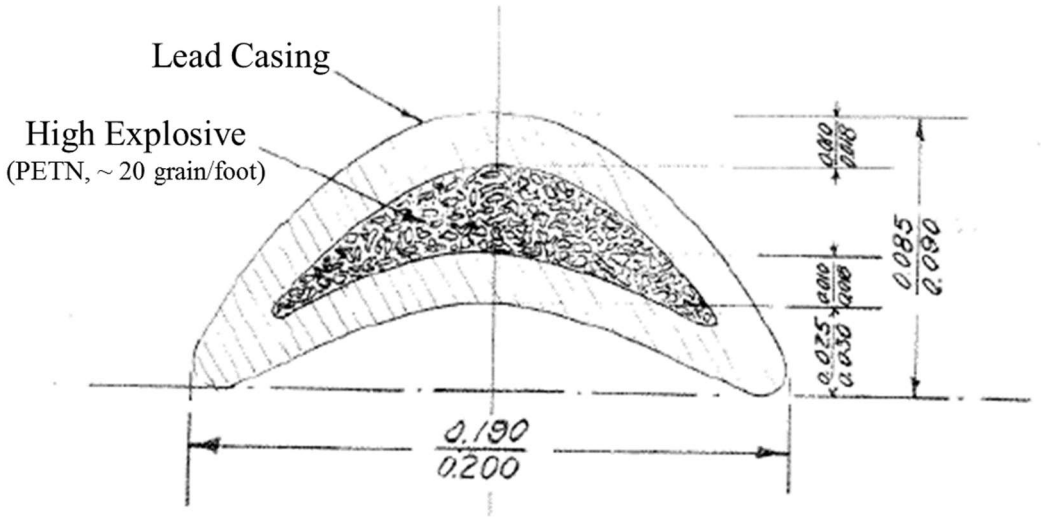

Figure 2.1 "U" Shaped Linear Shaped Charge. Adapted from [3]

Present day linear shaped charge design has evolved since 1957 with the help of detonation modeling. The CTH software developed by Sandia National Laboratories is one of the more prominent modeling programs that still exists today to aid in understanding how changes in the shaped charge design will affect shock wave propagation. Through the use of simulation software packages like CTH, variables such as apex angle and liner thickness have been able to be optimized to the designs typically seen today, as shown in Figure 2.2 [7, 8].

Figure 2.2 Linear shaped charges of various sizes. [9]

Since the advent of linear shaped charges, many advancements have been made that allow for greater penetration as well as ease of use, but the overall shape and design of the linear shaped charge has remained the same. As shown in Figure 2.2, current linear shaped charges have retained the overall concave shape as seen in Figure 2.1, however the shape has evolved into a “V” instead of a “U”.

Materials used as the liner for linear shaped charges have evolved from improved performance. Lead sheaths are seldom used as most linear shaped charge sheaths are now made of copper or even aluminum. The materials listed in Table 2.1 reflect the variety metals that can and have been used as material for liners, but potential liner materials are not limited to just metals. Glass, ceramics, and even water [10] can act as liners for shaped charges, if applied and setup properly.

Table 2.1 List of Potential Liner Materials for Conical Shaped Charges. Adapted from [11]

Face Centered Cubic Crystal (High ductility-good jets)			Body Centered Cubic Crystals (Low ductility-chunky jets)			Hexagonal Crystals (Powder jets)		
Element	Density (g/cc)	Melting Pt. (°C)	Element	Density (g/cc)	Melting Pt. (°C)	Element	Density (g/cc)	Melting Pt. (°C)
*Aluminum	2.69	660	Chromium	7.22	1890	*Beryllium	3.5	1278
*Copper	8.93	1083	*Iron	7.86	1535	Boron	2.34	2300
*Gold	18.98	1063	Lithium	0.53	186	*Cadmium	8.65	321
*Lead	11.34	327	Molybdenum	9.01	2620	*Carbon	3.52	3550
*Nickel	8.8	1455	Tantalum	16.6	2996	*Cobalt	8.71	1495
*Platinum	21.37	1773	Vanadium	5.96	1710	*Magnesium	1.74	657
*Silver	10.42	960				Osmium	22.5	2700
Tungsten (Beta)	19.3	3770				*Titanium	4.5	1800
						*Zinc	6.92	419
						*Zirconium	6.44	1857

Mixtures

Antimony-Lead

Glass

Aluminum-zinc

Aluminum-copper

Zirconium-tin

*Known to have been experimentally investigated

2.2. THEORY OF SHAPED CHARGES

Much research has been performed and literature has been written about conical shaped charges due to its prevalence in militaristic affairs, while comparatively little has been researched or tested regarding linear shaped charges. In fact, many simulators with linear shaped charge models do not accurately represent how the linear shaped charge functions which will be discussed in more detail in Section 2.2.2. In order to understand how linear shaped charges work, a basic understanding of the theories behind shaped charges is needed and will be covered in the follow subsections.

2.2.1. Fundamental Theories. Linear shaped charges are a smaller branch of the shaped charge family. All shaped charges exhibit some form of the Munroe effect. The underlying theory behind the Munroe effect is an explosive charge with a hollow void in it will produce more penetration depth into a target than an explosive charge without a hollow void. The intense pressures produced when the explosive is detonated is focused into a specific area, directly against the object of which the hollow void is pointing towards. When the hollow cavity of an explosive is lined with a layer of material, such as metal or glass, the depth of penetration becomes even greater than with a similar shaped explosive without the layer of material [12, 13]. Additionally, the penetration effect is further increased when the explosive charge with liner is moved a certain distance away from the intended target. This distance is known as the standoff distance. [1] Figure 2.3 depicts the relationships described above.

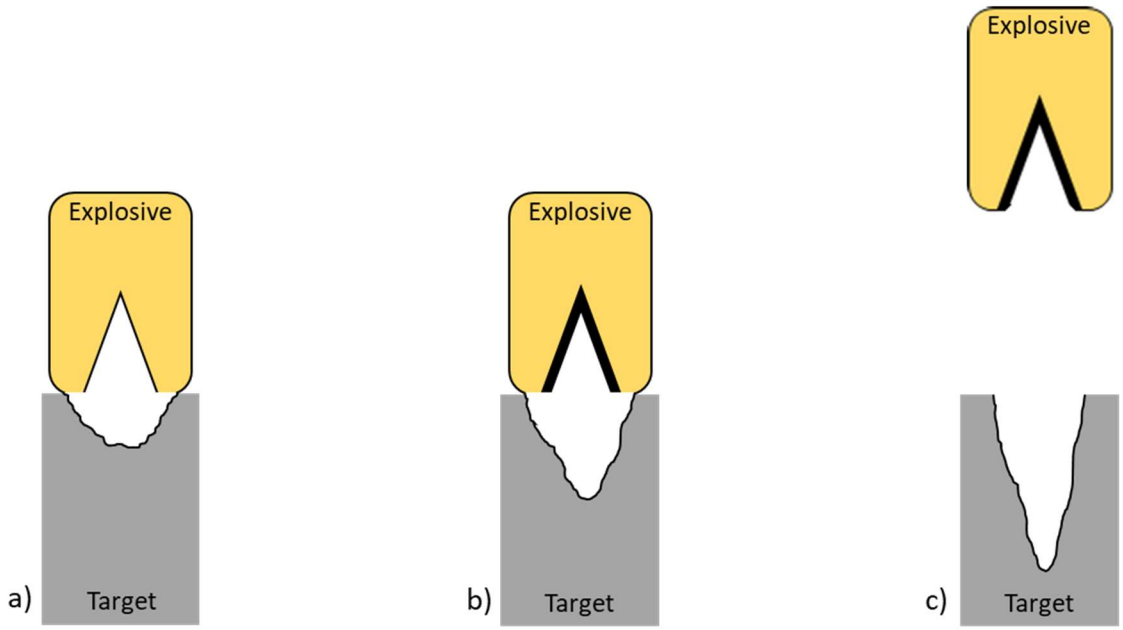

Figure 2.3. Comparison of explosive charges. a) explosive charge with void, b) explosive charge with void and liner, c) explosive charge with void, liner, and standoff. Adapted from [1]

As the explosive is initiated for a conical shaped charge, a shock front propagates radially through the explosive. This radial shock front eventually evens out into an almost planar shock front when it reaches the liner, causing the liner to collapse upon itself due to the extreme pressures caused by the explosive. During this collapse, a jet is formed by a fraction of the liner, due to the high pressure and high velocity caused by propagation of the explosive detonation. This jet extrudes outward and pushes through the target, resulting in penetration of the steel target. The standoff depicted in Figure 2.3 provides the time and space needed for the jet to fully form before reaching the target, which results in a deeper penetration depth.

2.2.2. Linear Shaped Charge Blade Collapse – Misznay-Schardin Effect. It has long been thought that linear shaped charges utilize the Munroe Effect to penetrate through their intended target. However, the research performed by Dr. Lim has disproven this theory [14, 15, 16, 17, 18]. Instead, the Misznay-Schardin effect is used to explain that the forces acting upon the lower V-shaped portion of the liner produces pressures that are perpendicular to the surface of the explosive. These pressures push upon the inverted "V" and the rest of the liner in a direction normal to the liner's faces, which causes spallation to occur at the edges of the liner. Because of the fractures occurring along the edges, the two sides of the inverted "V" collapse against one another, forming the blade that cuts down into the target [15].

To prove that the Misznay-Schardin effect was more in line with how a linear shaped charge functions compared to the Munroe effect, Lim suspended and initiated a linear shaped charge directly in the center of ¼ inch-thick steel pipe to catch the fragments, which allowed for the fragments and fragmentation pattern to be studied [14]. Four distinct indentations were discovered in the steel pipe, not including the area where the blade had penetrated through, created by fragmentation from the linear shaped charge. The locations of these indents were directly perpendicular to the external flat sides of the linear shaped charge. Refer to Figure 2.4 for an image of the results of the "pipe test" [14].

To confirm the source of the additional indents, a custom J-shaped linear shaped charge was created with one and a half sides of the linear shaped charge exposing the explosive material, as shown in Figure 2.5 [14].

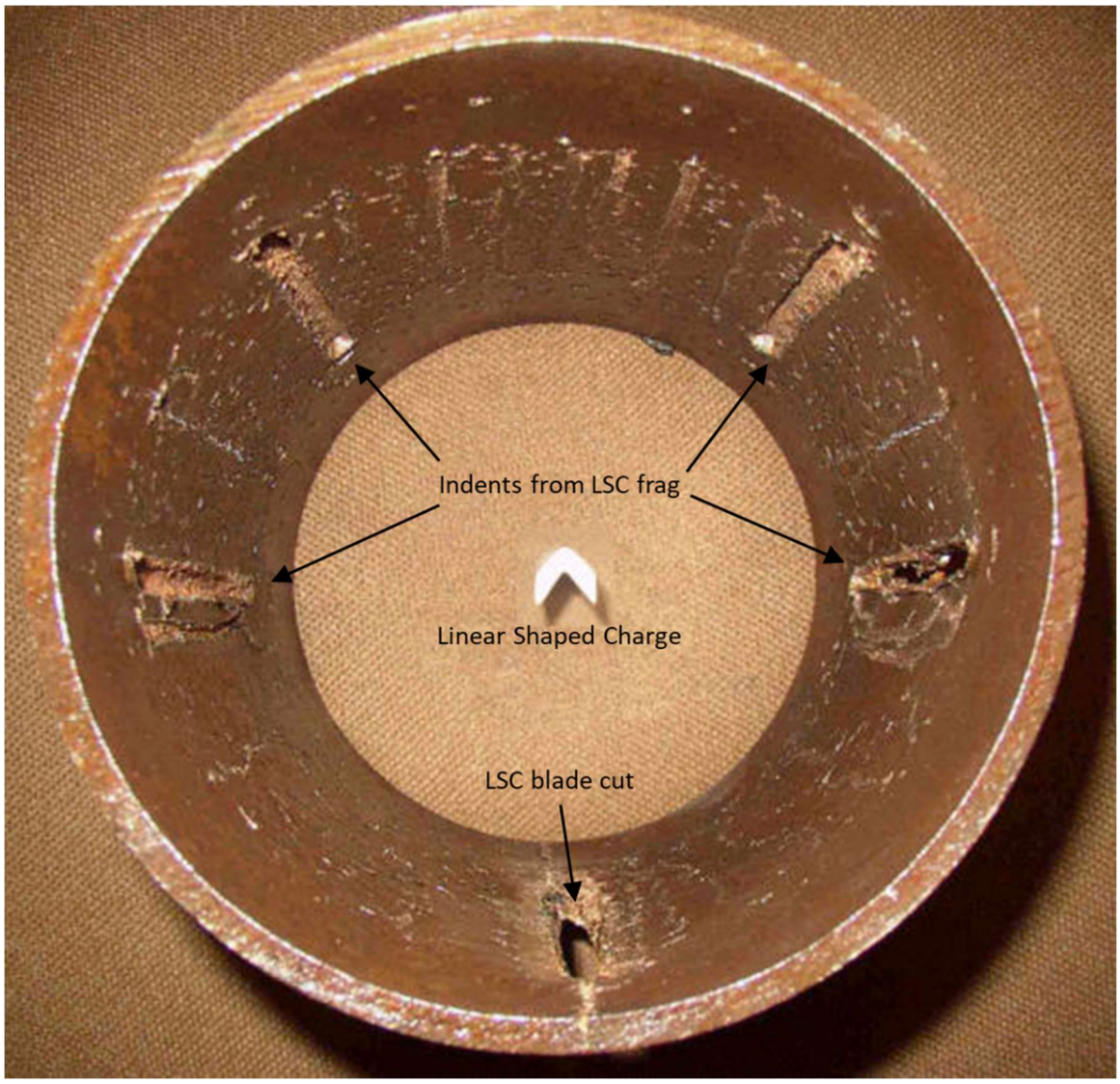

Figure 2.4 Fragmentation result of pipe test. An unused linear shaped charge is placed in the middle of the steel pipe to depict the position of the liner shaped charge prior to detonation. Adapted from [14]

The resulting fragmentation pattern caused by the shrapnel of the J-shaped linear shaped charge shows three distinct indentations directly perpendicular to the flat “sides” of the J-shaped linear shaped charge. The size of the indentations is proportional not only

to the amount of copper sheath material available on each side, but also to the amount of confinement available.

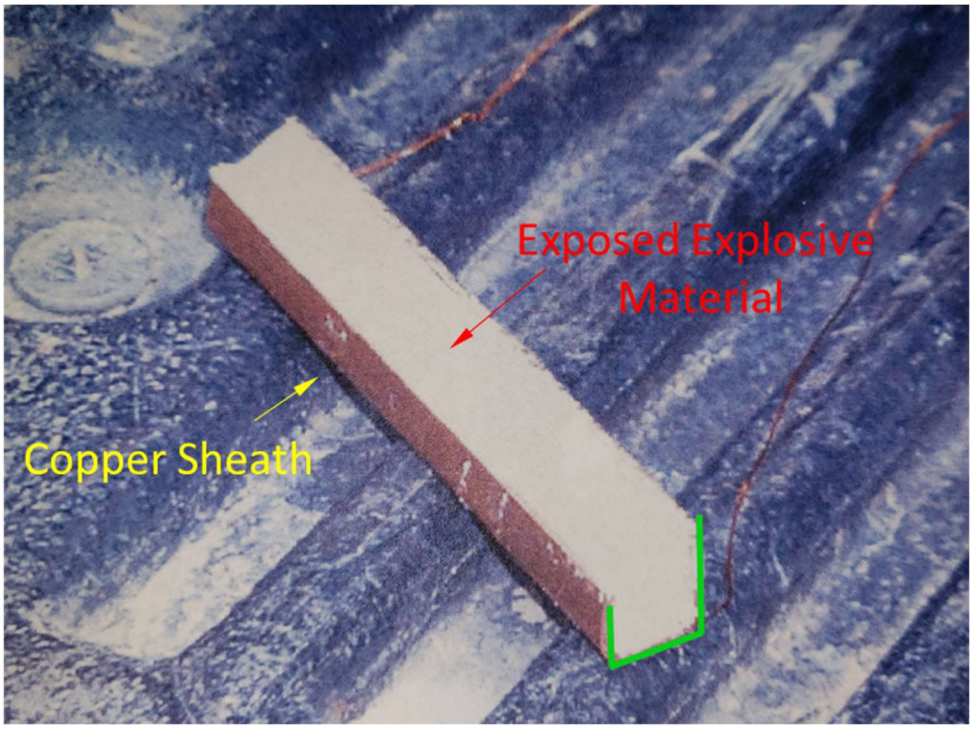

Figure 2.5 J-shaped linear shaped charge. Adapted from [14]

The largest indentation, shown in Figure 2.6, is opposite the only side of the J-shaped linear shaped charge that has confinement from the two other sides. It is noticeably wider and deeper than the other two indentations. The smallest and most shallow indentation corresponds to the shortest side of the J-shaped linear shaped charge. This side was only half the height of either of the other two sides. Of note is the lack of any fragmentation pattern within the area of the pipe that was facing the exposed explosive material. The sides of the pipe that had sheath from the J-shaped linear shaped

charge facing them are peppered with shrapnel, which sharply contrasts with the lack of shrapnel in the exposed explosives side.

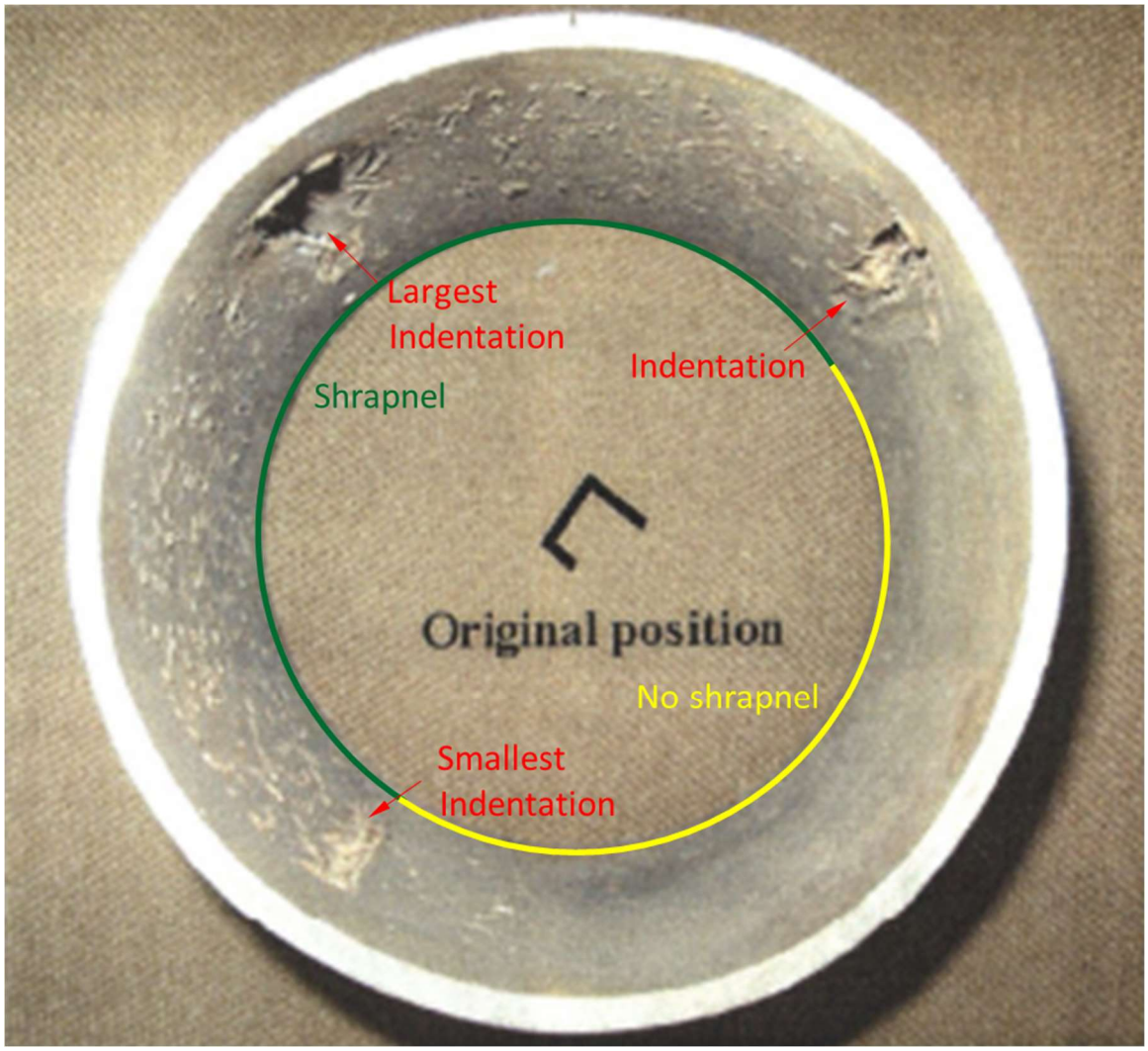

Figure 2.6 Fragmentation result of J-shaped linear shaped charge testing. Adapted from [14]

Lim performed further research into the linear shaped charge blade collapse with the use of a Cordin camera to capture exact moments of a linear shaped charge initiation.

The images taken resulted in showing the inverted “V” section of the liner collapsing together. Refer to Figure 2.7 for an image taken during the initiation of a linear shaped charge.

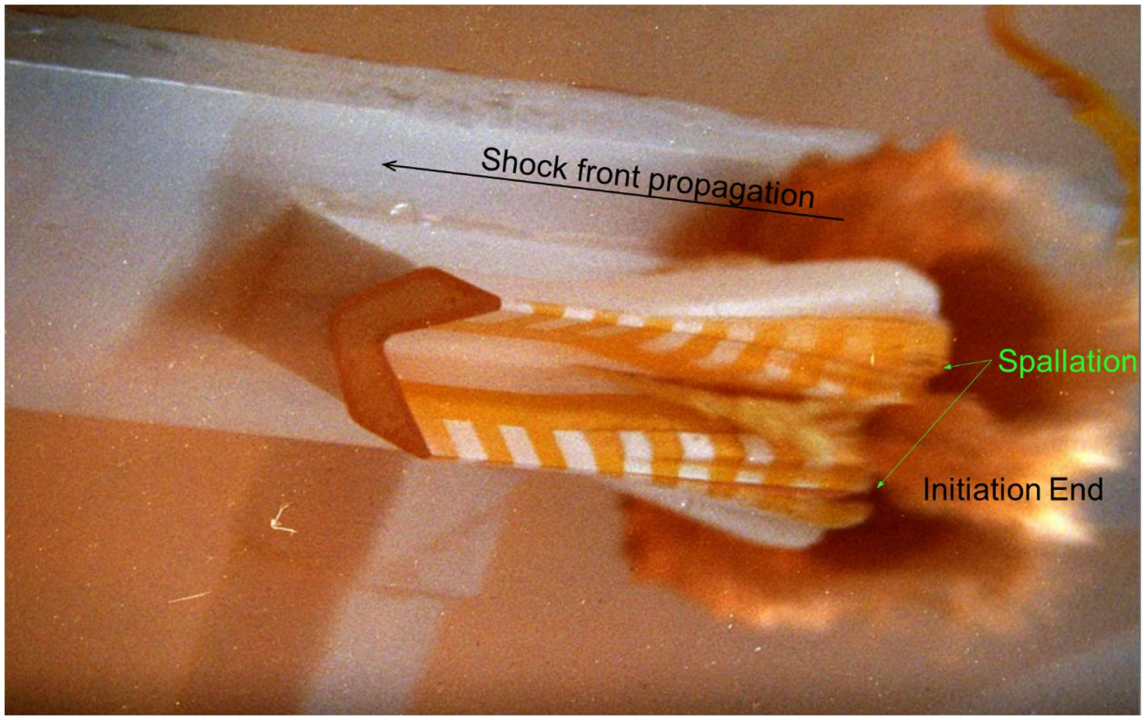

Figure 2.7 Image of linear shaped charge initiation captured by a Cordin camera. Photo taken courtesy of Dr. Lim

It was also discovered that spallation occurs almost immediately at the vertices of where the inverted “V” section meets both vertical sides of the liner [15]. The fractures have already split the sections at the initiation end and continue to form as the shock front propagates through the linear shaped charge. The other end of the linear shaped charge

shows no change in the image, therefore it can be surmised that the fractures occur and break off almost immediately, given the velocity of detonation of the explosive.

Further testing has been performed on the formation of the linear shaped charge blade including underwater testing [19]. It was discovered that the water hindered the collapse of the liner, thus the blade never closed and fully formed.

2.2.3. Optimal Shaped Charge Design. The following variables of linear shaped charges were identified and characterized on how they affect the cut: 1) size (grains per foot) of the linear shaped charge, 2) standoff distance, 3) run up and run down area (Please refer to Section 2.2.4 for more detailed information regarding run up and run down), 4) size and location of the primer (initiation device) charge, and 5) shrapnel patterns [14].

Based on the Sandia national lab's SCAP report for conical shaped charge liners, the optimal apex angle at which maximum penetration depth had been achieved was at 42° [7]. Other factors such as liner thickness, liner composition, amount of explosive used, type of explosive used, confinement of the shaped charge, and standoff distance also contributed to the effectiveness of the shaped charge as well as the depth of penetration [7]. Sandia's testing revolved around conical shaped charges, so some of the data does not directly translate to linear shaped charges as shown previously in 2.2.2, but the basic concepts such as apex angle, liner thickness, and liner material apply to both conical and linear shaped charges.

The researchers at Sandia also performed tests comparing penetration depth of conical shaped charges with different liner materials. They theorized that higher densities of liner material with respect to the target density will result in greater penetration. They

compared the penetration results between a liner made from copper and a liner made of from steel. Based on their results, shown in Figure 2.8, copper liners consistently produced greater penetration compared to steel liners.

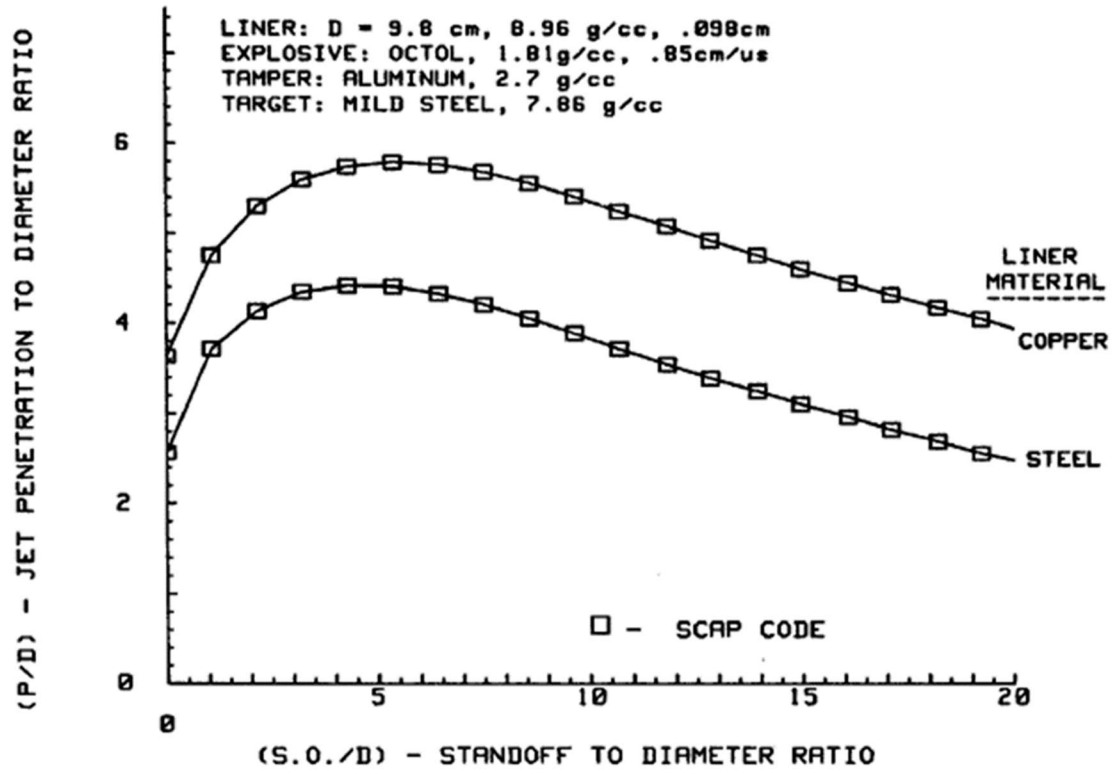

Figure 2.8 Depth penetration comparison between copper and steel conical shaped liners. [7]

2.2.4. Run Up and Run Down Phenomena. Run up and run down are phenomena that regularly occur with the use of linear shaped charges. Run up refers to the area in the initial stages of the target where the depth of penetration is constantly increasing until it reaches the steady state penetration depth and stabilizes. Run up is primarily due to the shock front propagating radially away from the point of initiation. The shock front rapidly flattens out into a planar wave as it travels through the LSC, at which point maximum penetration is achieved and the depth of penetration stabilizes.

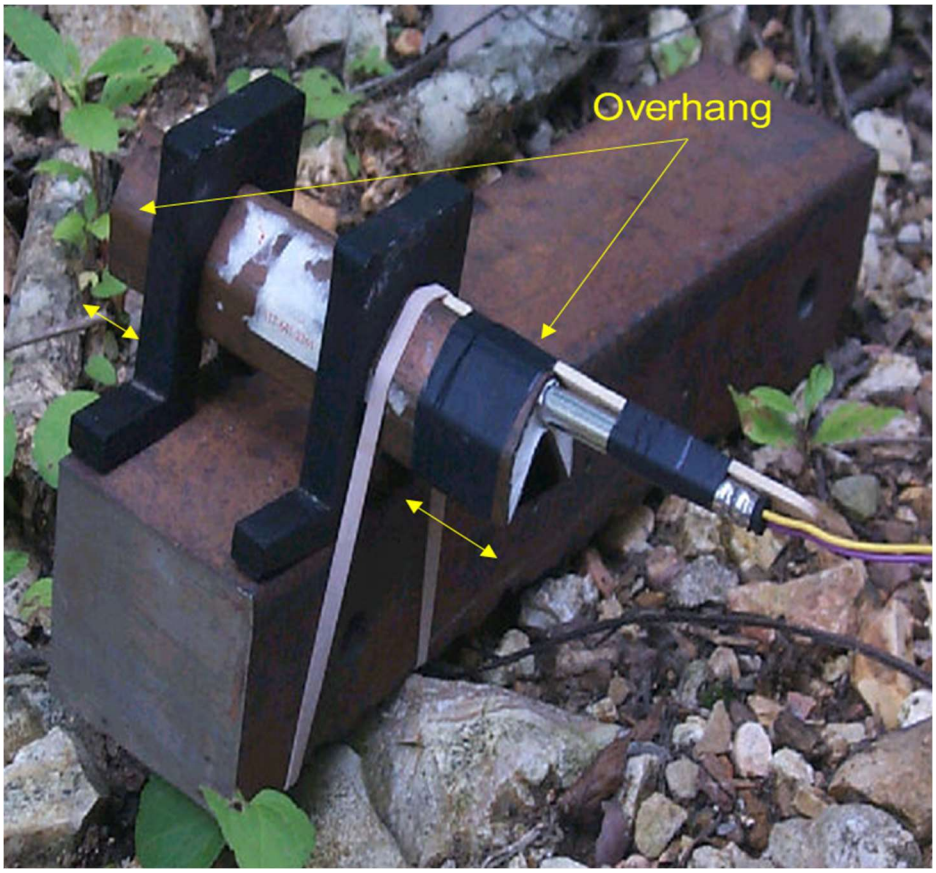

Figure 2.9 LSC setup with proper overhang.

Run down refers to the area at the end stages of the target where the depth of penetration decreases rapidly from the stable penetration zone. Run down could be caused by the lack of confinement at the end of a linear shaped charge. The confinement of the liner directs the explosive pressure steadily in the downward direction, but with no confinement at the end, all of the explosive energy exits into open space and there isn't a constant force cutting into the target anymore. To account for the run up and run down phenomena during conventional use, the linear shaped charge must be longer than the intended cut in order to cut cleanly through, as shown in Figure 2.9. Figure 2.10 displays the run up and run down phenomenon from the results of linear shaped charge testing [14].

Lim discovered the run up and run down areas to always exist whether using conventional or commercial linear shaped charges. The size of the run up distance often differed based on the size of the explosive charge itself, with the run up distance being longer if the linear shaped charge was a larger grain per foot size. A correlation between maximum depth penetration and run up distance was observed as well. When the run up distance results from the various sized charges were compared with each other by normalizing all results to the 500 grain per foot linear shaped charge, the run up distance was found to be constant. Results from the primer size and initiation location testing also proved to affect the run up to a certain degree; a clear trend was seen with a larger primer size equating to a shorter run up distance [14].

Based on data acquired through testing done by Nolan, et al. [20] and Ortel [21], the run up effect occurred in the initial third of the length of the LSC. In a similar vein, run down refers to the area in the latter stages of the target where the depth of penetration

decreases. Run down may be due to a combination of the lack of confinement at the end of the LSC in which much of the energy disperses out the open end, as well as running out of explosive material to continue to propagate the shock front.

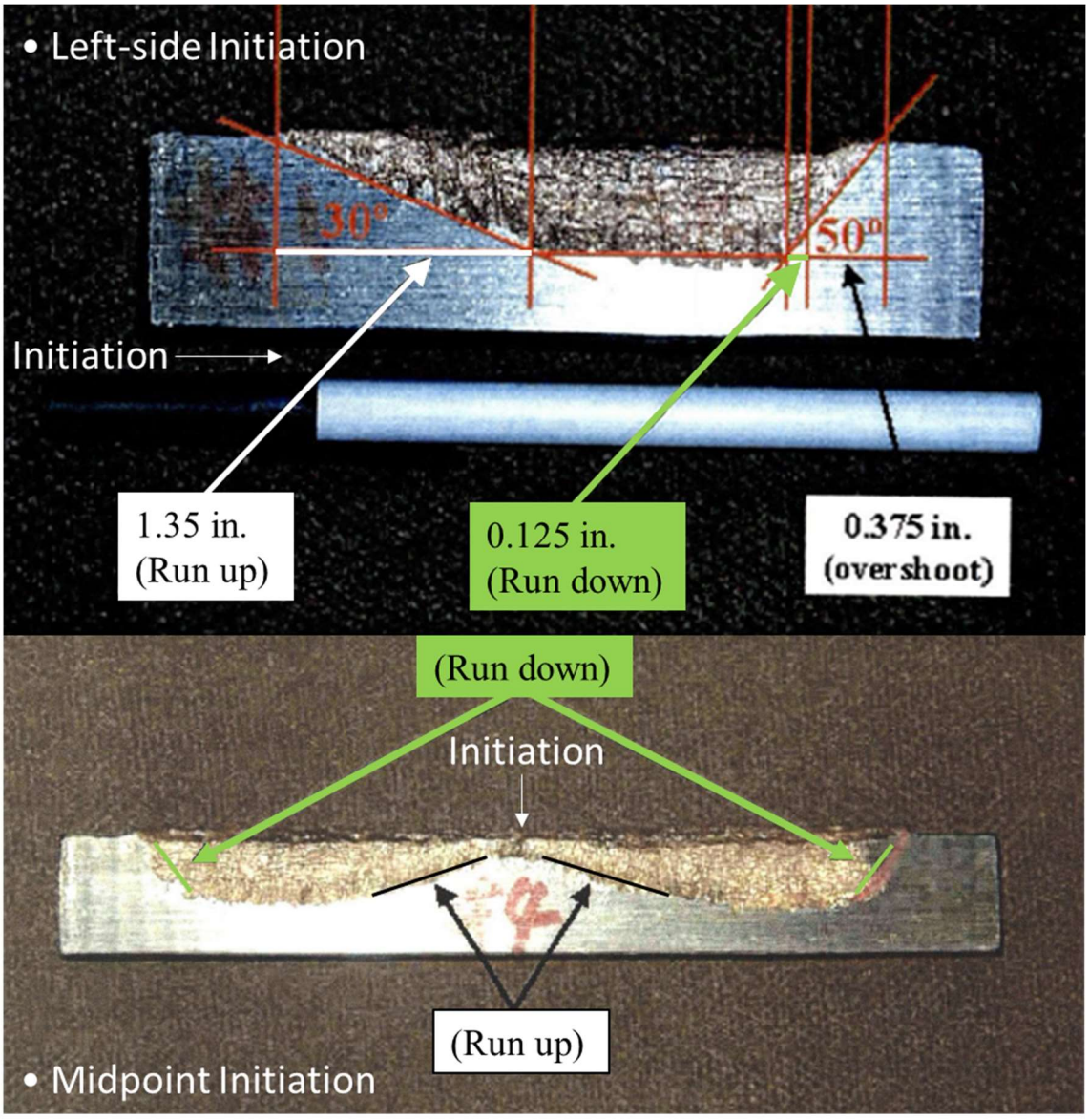

Figure 2.10 Images of targets cut in half, depicting run up and run down. Left-side Initiation: run up zone is highlighted in white and run down zone is highlighted in green. Midpoint Initiation: run up zone is highlighted in black and run down zone is highlighted in green. Adapted from [14].

2.3. ADDITIVE MANUFACTURING

Additive manufacturing is the process of building three dimensional objects layer by layer. Traditionally, manufacturing objects is a subtractive process, where an object is shaped by removing material from the object through machining, carving, milling, or any other means possible. Additive manufacturing allows for geometric complexity not possible with traditional manufacturing techniques. Additive manufacturing relies on computer-aided-design (CAD) software to design and create an object. The CAD data is then transferred to the printing machine, where it fabricates the object to its exact dimensions, layer by layer, until the final product is completed. This section discusses different additive manufacturing processes available and touches upon the pros and cons of utilizing these processes to produce linear shaped charge liners.

2.3.1. Types of Additive Manufacturing. There are seven different types of additive manufacturing as defined by the International Organization for Standardization (ISO). ISO in conjunction with ASTM International, formerly known as American Society for Testing and Materials, developed ISO/ASTM 52900 document, intending to create a common set of standards for additive manufacturing [22]. The seven types of additive manufacturing are as follows: binder jetting, directed energy deposition, material extrusion, material jetting, powder bed fusion, sheet lamination, and vat photopolymerization. Within each type of additive manufacturing, there can be several different techniques used to manufacture parts or components.

Each type of additive manufacturing has different pros and cons as well as different materials used as their building substrate. Additive manufacturing types vat photopolymerization, material extrusion, and material jetting often use polymers or

plastics as their main building substrate [23]. The build process consists of using light or heat to mold the resin or plastic material into the shape desired. These types of additive manufacturing processes often have quicker build times of the components than some of the other types, but the structural strength of the final product is not conducive to producing reliable results for testing high explosives.

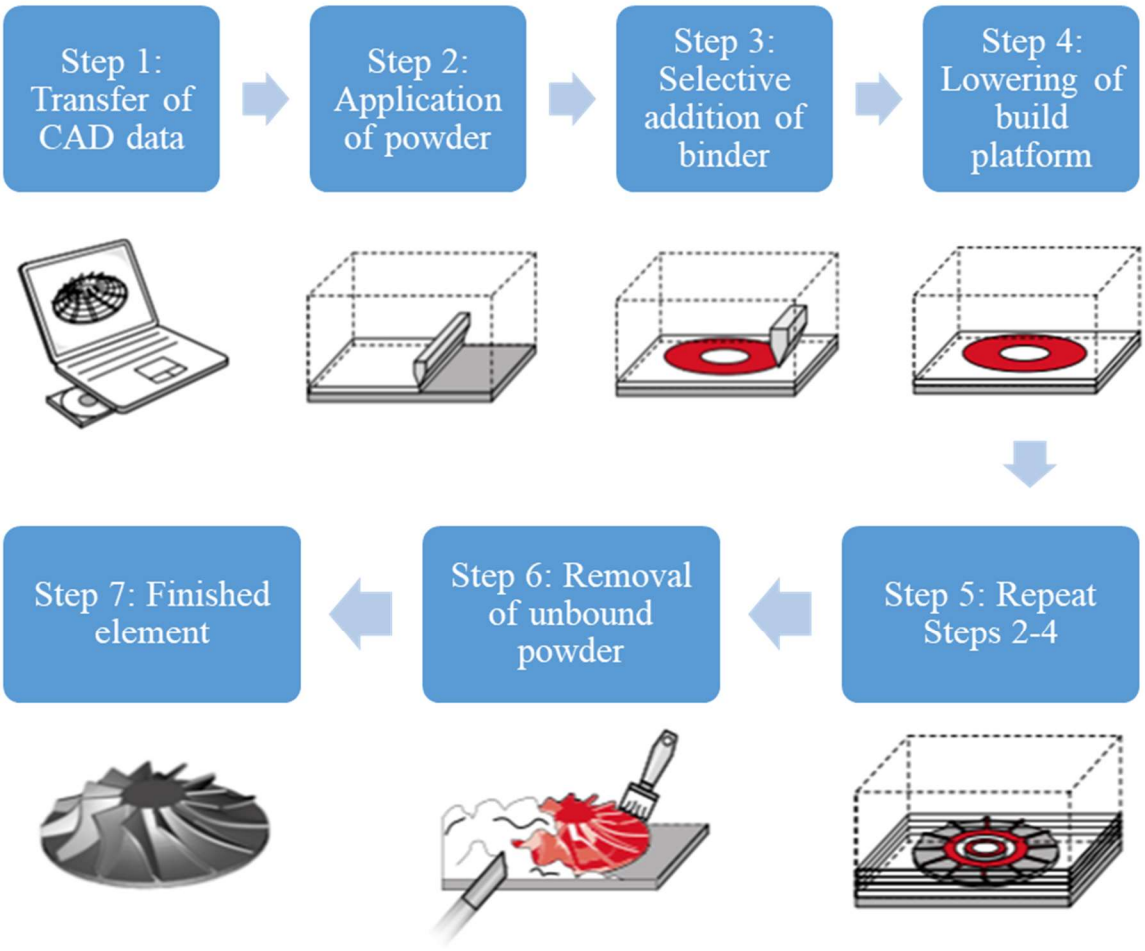

Figure 2.11 Flow chart of binder jetting process. Adapted from [24]

Binder jetting and sheet lamination rely on utilizing binding agents to hold together the layers of the build [23]. Figure 2.11 displays the general steps taken during the binder jetting process.

The strength of the binding agent ultimately becomes the basis of the structural integrity of the additively manufactured part. Having to rely on the strength of binding agents while testing at the high pressures and temperatures associated with high explosives is also not an ideal condition to collect reliable and consistent data.

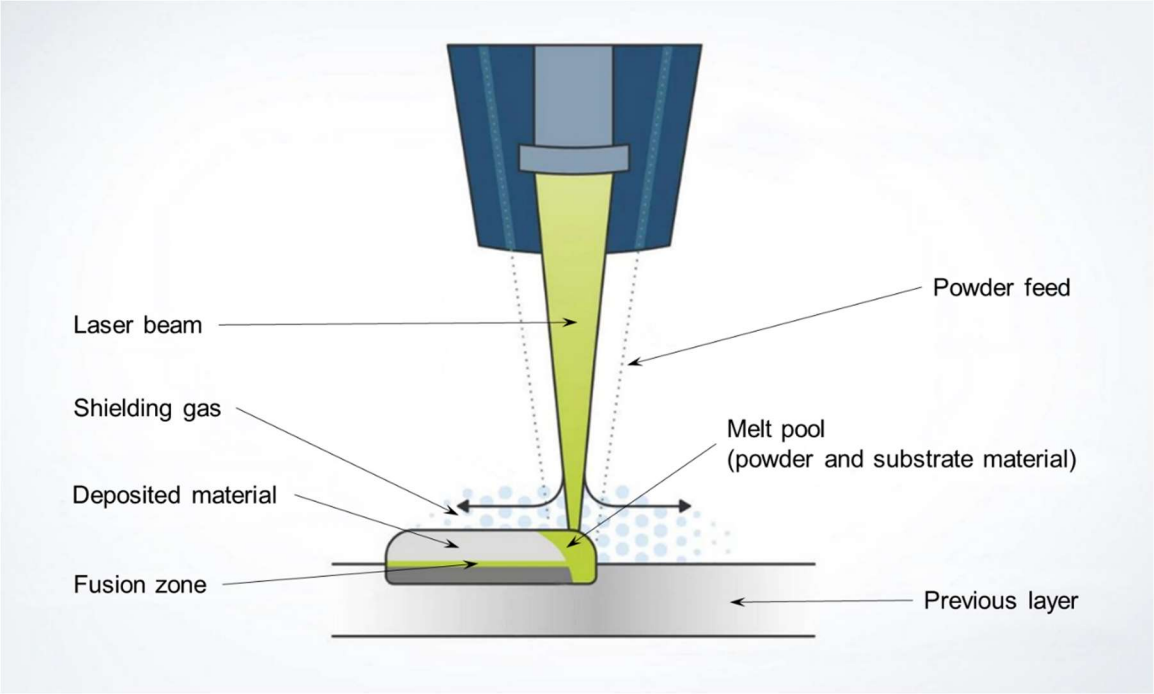

Figure 2.12 Schematic of directed energy deposition process. Adapted from [25]

The last two types of additive manufacturing are directed energy deposition and powder bed fusion. While powdered materials such as polymers or ceramics can be used

by both types of additive manufacturing, powdered metals are predominantly used instead. Both of these processes melt the substrate such that the melting material fuses with the substrate, creating a structural bond that is formed on a molecular level between each layer. The main difference between directed energy deposition and powder bed fusion is directed energy deposition melts the substrate area together with a continuous feed of the melting material and deposits the melting material on top of the previous layer, while powder bed fusion spreads out an entire layer of powdered melting material before proceeding with melting the layer onto the previous layer. [23] Figure 2.12 and Figure 2.13 display schematics of the general process of directed energy deposition and powder bed fusion, respectively.

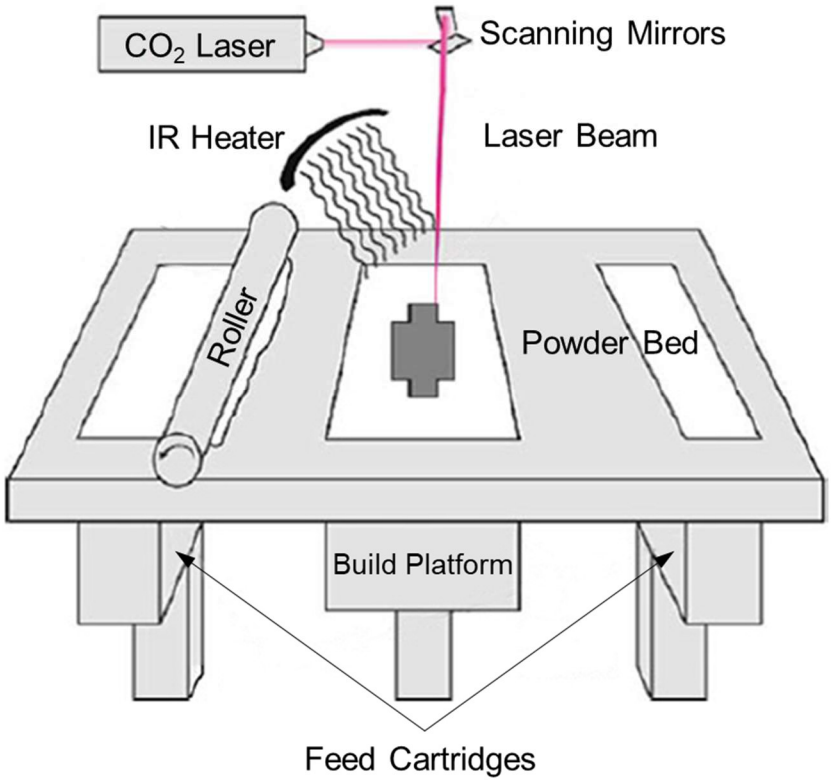

Figure 2.13 Schematic of powder bed fusion process. Adapted from [23]

While both directed energy deposition and powder bed fusion provide adequate building materials and construction of parts to use in testing with high explosives, a few key differences between the building processes make powder bed fusion the ideal additive manufacturing choice to create liners for shaped charges. In the directed energy deposition process, there is little or no support structures or build plates, so the more complex geometries cannot be built as these often require a dense network of support structures. The directed energy deposition process also creates a larger melt pool area when fusing, which diminishes its accuracy in creating those complex, small-scale geometries when compared to the powder bed fusion process. In fact, the area of expertise that the directed energy deposition process excels in is one of a kind amongst all the additive manufacturing types; the repair and "addition of features" area. Because of the lack of support structure or a building base, directed energy deposition is generally used to either add on to an already existing part or component, or directly repairing a cracked or broken object, as shown in Figure 2.14. [23] To build the parts of a shaped charge liner from base to top, it would seem to be best to utilize powder bed fusion as the additive manufacturing choice.

Figure 2.14 Directed energy deposition. [25]

2.3.2. Powder Bed Fusion and Selective Laser Melting. There are several different techniques used within the archetype of powder bed fusion, categorized by the energy source used to melt the powdered materials: thermally fused, laser fused, electron beam fused, fused with agent and energy. The actual processes' names may vary based different companies utilizing trade-terms, but the most common names of these techniques are selective heat sintering (thermally fused), selective laser sintering and selective laser melting (laser fused), electron beam melting (electron beam fused), and multi jet fusion (fused with agent and energy) [26]. A variety of materials and alloys can be processed by powder bed fusion including stainless steels [27, 28], titanium alloys [29], superalloys [30], thermoelectric materials [31], and shape memory alloys [32, 33, 34]. Figure 2.15 displays a flowchart of the various powder bed fusion techniques.

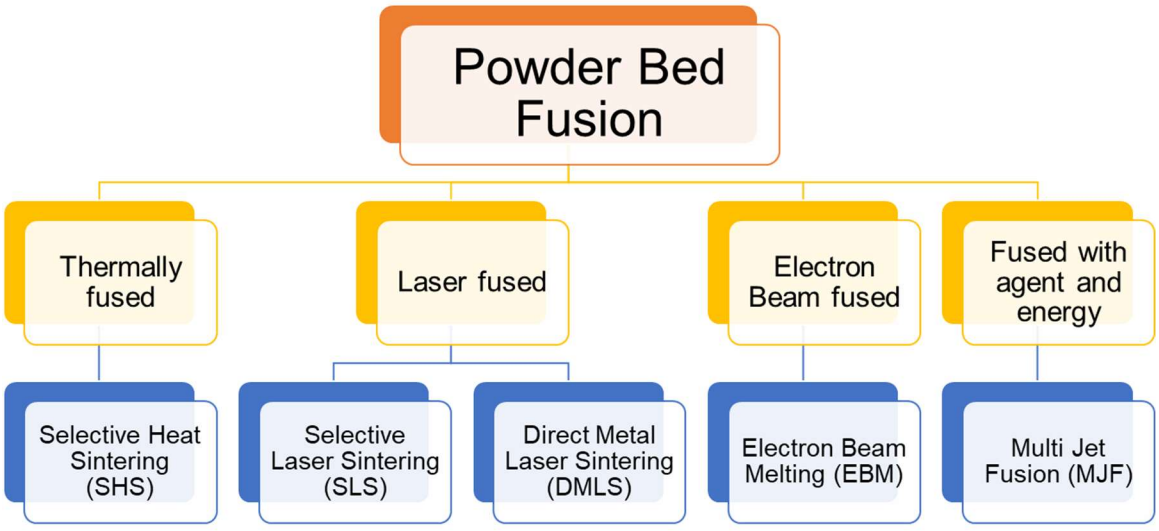

Figure 2.15 Powder bed fusion flowchart. Adapted from [26]

For the purposes of creating and manufacturing metal-based liners, selective laser sintering and selective laser melting are both capable of performing the task. The main difference between selective laser sintering and selective laser melting is selective laser sintering heats the powder to the temperature at which the powder fuses together on a molecular level, whereas selective laser melting fully melts the powder together such that the end result is completely homogenous. [35] [36] Compared to selective laser sintering, the selective laser melting process creates a final product more closely resembling machined linear shaped charge liners. The density of the resulting component is capable of reaching 99.9% bulk density of the metal used, depending on the energy output of the laser. [37] Testing was done to compare the performance between conical shaped charge liners that were machined and conical shaped charge liners that were additively manufactured and filled with the high explosives composition C-4. Both sets of liners were created from the same basic material, 304L stainless steel, and the geometries of the liners were identical. The testing resulted in 7 witness plates being penetrated by both the machined and additively manufactured liners and demonstrated that the additive manufacture process can be applied to shaped charge liners with repeatability [38].

2.4. SUMMARY

Through analysis and research of literature reviews done in Sections 2.1, 2.2, and 2.3, the following conclusions have been arrived at to form the basis of the methodologies used in thesis:

- Run up and run down will occur in a target cut by a linear shaped charge, regardless of the size of the charge and the initiation locations.

- The apex angle of a shaped charge has a profound effect on the depth of penetration produced by the shaped charge.
- Confinement of explosive energy, however temporary, will direct the majority of the energy towards the path of least resistance.
- Steel liners will overall produce less penetration than copper liners due to structural composition.
- Powder bed fusion additive manufacturing, specifically utilizing the selective laser melting technique, will provide the most efficient and effective way of creating custom liners to test with for linear shaped charge testing.

3. LINEAR SHAPED CHARGE DESIGN AND METHODOLOGY

This section details the concept, design and manufacture of the custom LSC liners. It will also contain the methodology used to test the custom LSC liners for the reduction of run up and run down. A Renishaw AM250 selective laser melting system was used to manufacture the LSC liners with 304L stainless steel powder. The consistency of the printed liners was 99% density bulk 304L. Composition C4 was used as the explosive to perform testing with. All tests were conducted according to the safety rules at the mine by trained personnel.

3.1. 3D-MODELING OF THE LINEAR SHAPED CHARGE

The dimensions of a commercial, copper-based, 1200 grain linear shaped charge were measured to serve as a basis for modeling the additively manufactured linear shaped charge liner. The actual dimensions and their corresponding placements are displayed in Table 3.1 and Figures 3.1 and 3.2.

Table 3.1 Linear Shaped Charge Dimensions [39]

Linear Shaped Charge	Width (in, ± 0.03)	Height (in, ± 0.03)	Base Apex Angle	Top Apex Angle
Commercial Model	0.92	0.90	85°	94°
CAD Design	0.89	0.90	85°	94°

The computer-aided design (CAD) software, Solidworks, was used to design and create the testing components from scratch. Solidworks also allowed for entire assemblies

to be fabricated by combining different parts together. The parameters listed in Table 3.1 were input into the CAD program to create the liner models. Constraints and restrictions can be embedded or set into every line, face, or angle such that the component created is the proper size and shape required, as shown in Figure 3.1 and Figure 3.2.

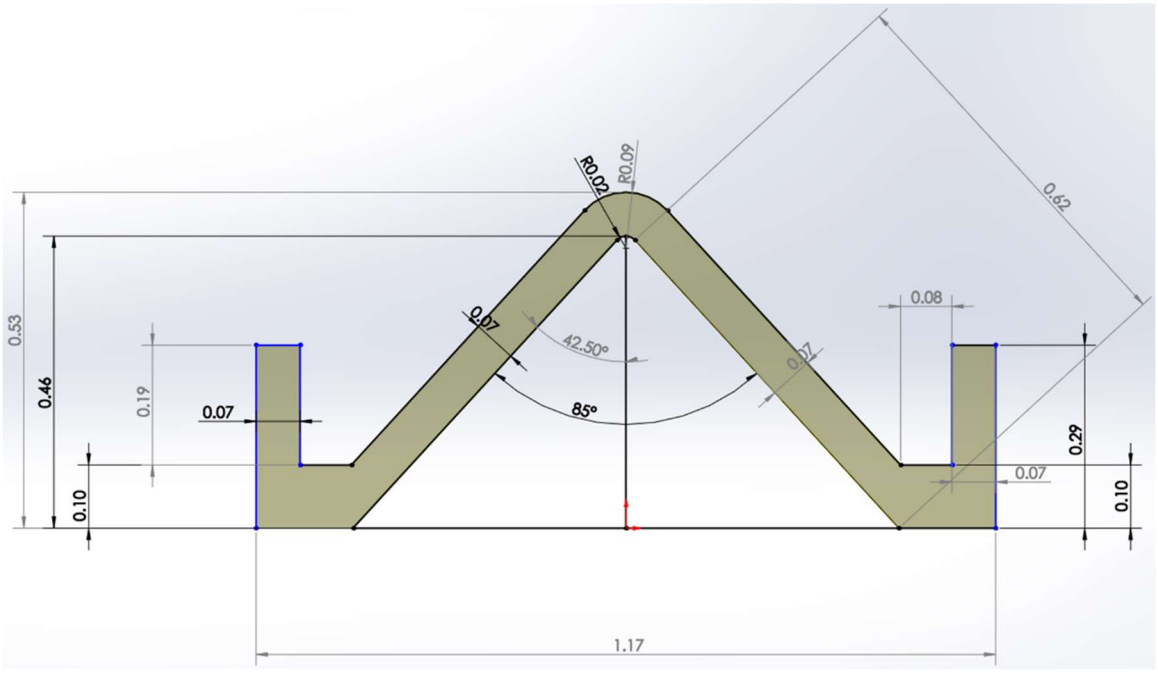

Figure 3.1 Schematic of an LSC base liner with detailed measurements in Solidworks [40].

Once dimensions were finalized, the file is output as a stereolithography file to run in a 3-D printing program, Materialise Magics, for use with the Renishaw AM250 printer. The 3-D printing program divides the CAD drawing into many thin layers in order to generate the slice data required for printing the components. This allows the selective laser melting machine to build the component layer by layer.

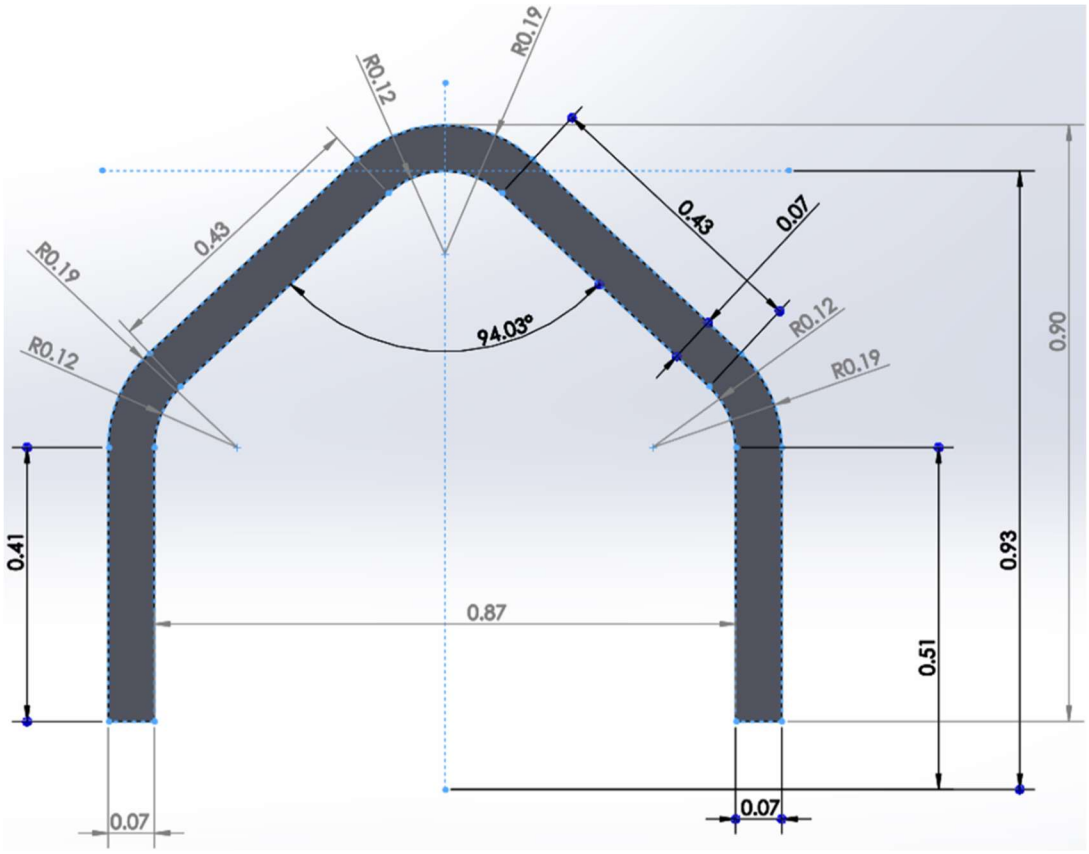

Figure 3.2 Schematic of an LSC top liner with detailed measurements in Solidworks [40].

Finally, the processed stereolithography files are uploaded to the selective laser melting machine for construction of the component. The machine starts with a thin layer of the metal powder on the build plate. A high energy laser then melts and fuses together the metal powder in specified areas according to the design file. Once all areas have been melted and fused together for the first layer, a new layer of metal powder is laid across the build plate and the process is repeated. This process continues until the component has been created to completion, as shown in Figure 3.3.

Figure 3.3 Finished linear shaped charge liners on build plate awaiting separation.

The energy output of the laser can be adjusted to lower the density of the component while still retaining the same overall structure, but for the testing purposes required, the laser energy settings were optimized to maximize density of the material. The thickness of the liner remained constant throughout the length of the LSC at 0.7 inches.

3.2. METHODOLOGY TO REDUCE RUN UP

The first test series was designed to examine the effect of altering the apex angle has on run up and whether the amount of run up could be reduced. To achieve this, the initial apex angle was reduced from the measured 85° (as previously stated in Table 3.1) to 70° and 55° to test if a more acute apex angle would produce a deeper initial cut to offset the run up effect and achieve maximum penetration at an earlier stage as part of hypothesis 1a. The apex angles of 70° and 55° were chosen for two reasons. The first is

in reference to the results from the SCAP Sandia report (Section 2.2.3) highlighting the fact that the more acute the apex angle was, the deeper the penetration result [7]. The second reason is because by designing an acute apex angle but keeping the remainder of the liner shell the same, there is a higher explosive material to liner ratio at the initiation end. The combination of more explosives pushing a more acute angle together would lower the amount of time and energy needed to create the blade.

One LSC was created to be the reference liner, with a length of 9 inches and an apex angle of 85°. The length of the LSC was limited by the print bed dimensions of 10" x 10" of the additive manufacturing machine, the Renishaw AM250. Two more separate LSCs were fabricated with apex angles of 70° and 55° at the initiation end, and were gradually extended back to the base reference of 85° over the initial 3 inches of the liner, as shown in Figure 3.4.

Each LSC consisted of two separate parts, the top liner and the base liner. Composition C-4 (C4) was hand-packed into the top liner of each LSC and molded to fit with the base liner with minimal space between. A mass of 89.31 grams was used to achieve an average target density of 1.6 g/cm^3 of C4, which would give a comparable amount of explosive to the referenced 1200-grain/foot copper LSC [39]. While the decrease in the apex angle consequentially increased the volume within the LSC, the overall change in mass to maintain a 1.6 g/cm^3 density of C4 was small, just under 3% difference between the mass of C4 for the 55° LSC and the 85° LSC. With minimal differences in explosive mass, any deviation that may occur due to this difference was deemed negligible for testing purposes.

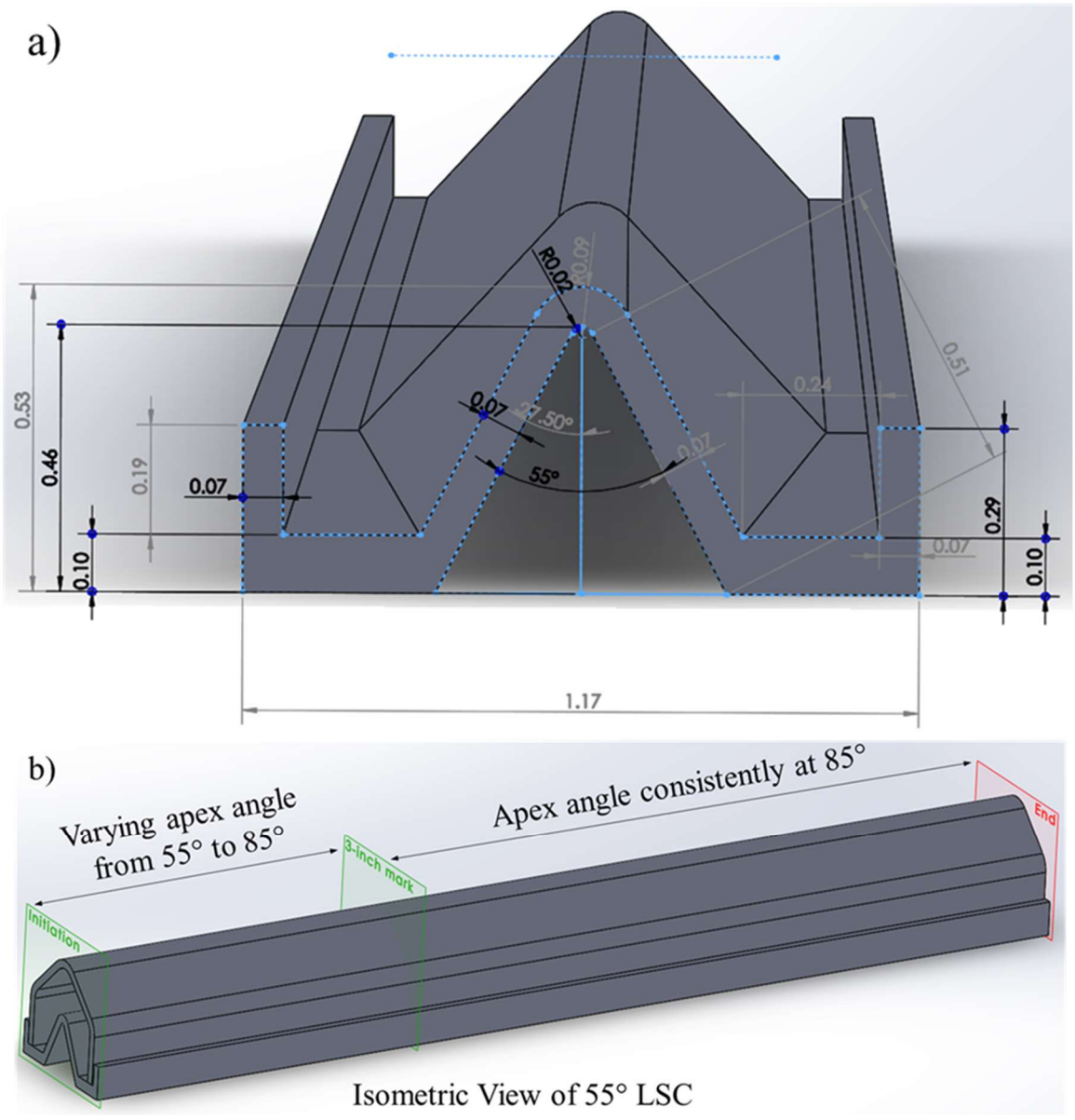

Figure 3.4 Solidworks model of 55° LSC. a) Front-to-back view of LSC base liner. Apex angle starts at 55° at the initiation end and gradually widens out to 85° at the 3-inch mark, where it remains at a constant 85° for the remainder of the liner. b) Isometric view of full LSC.

Hose clamps were fastened along the ends of the LSC to securely hold the charge together during testing setup but broke easily under explosive loading and did not impede

penetration. Each LSC was initiated with a standard #8 electric detonator connected to an 8g pentolite stinger to deliver a strong, consistent detonation wave to initiate the LSC. A foam standoff of ¾ inches based on published recommended standoff values [39] was used between the LSCs and the target, a 1 ½ inch mild steel target plate. Figure 3.5 depicts a partial set up of the experiment with standoff visible while Figure 3.6 depicts the full setup just prior to blasting.

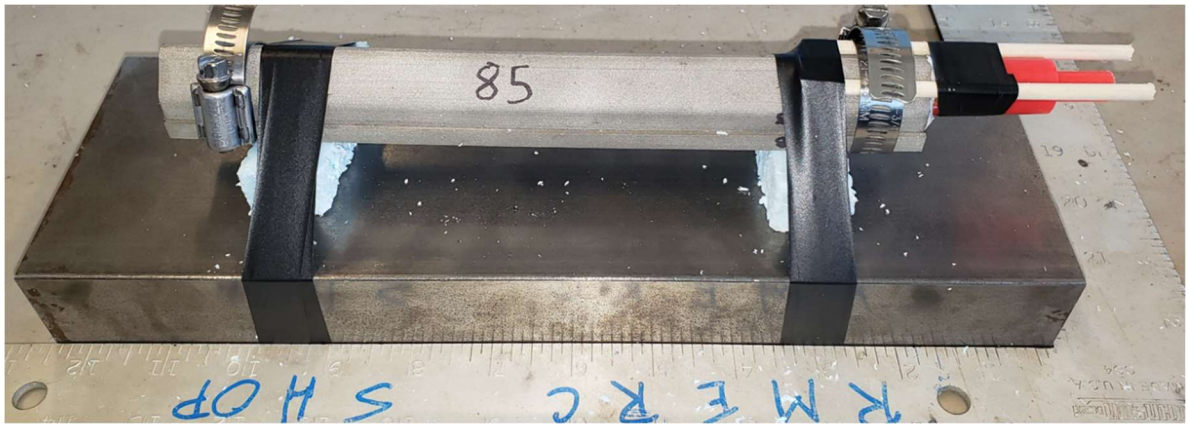

Figure 3.5 Side view of 85° LSC on top of 1 ½“ steel target. 8g stinger is used to ensure full shock front propagation is achieved. Styrofoam standoffs are ¾” high.

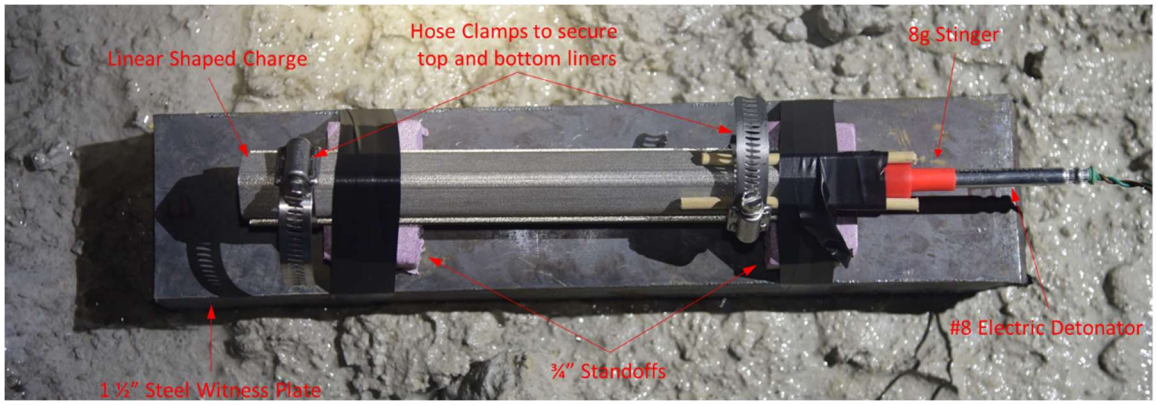

Figure 3.6 Full setup of experiment prior to initiation.

Blast testing was performed in a remote, underground area of the Wombat Mine to contain any fragments that resulted from the blast. Following the blast, the ventilation system was turned on to help vent the fumes from the explosion, and a full 20 minutes elapsed before the target plates were retrieved from inside the mine. Each of the resulting steel target plates were washed, sliced in half down the middle of the cut made by the LSC with a water jet, lightly buffed, and coated with a thin layer of clear acrylic paint to prevent further rust build up, as shown in Figure 3.7. Table 3.2 lists the parameters of each liner that was tested for this experiment.

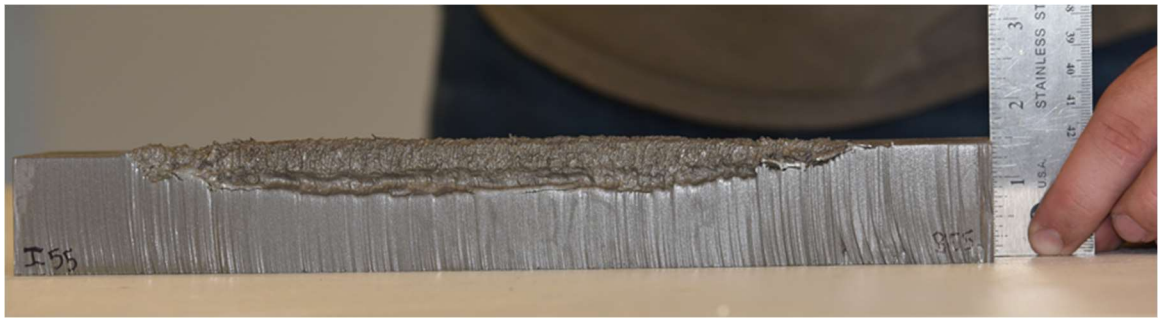

Figure 3.7 Steel target plate cut in half, buffed, and coated to perform analysis on.

Table 3.2 Testing Parameters of Run up Experiment. *Volumes of LSC were calculated within Solidworks.

Test	Mass of C4 (g)	Volume of LSC (cm^3)*	Density of C4 (g/cm^3)	Initial Apex Angle
1	89.30	55.82	1.600	85
2	90.75	56.70	1.601	70
3	91.70	57.35	1.599	55

3.3. METHODOLOGY TO REDUCE RUN DOWN

The second test series addressed reducing the run down compared to a traditional liner. To achieve this, a backstop was implemented into the LSC liner top to attempt to contain the explosive energy and reduce the run down effect.

The design for the LSC liner was based on measurements taken from a commercially available LSC, same as in Section 3.2. For this test series, a consistent 85° apex angle was used for all liner bases, the overall length of the liners were 9 inches long, and an additional backstop with varying degrees of thickness was added to the liner tops. The backstop thickness was determined according to overall liner thickness; one, two, and three times the overall liner thickness of 0.7 inch, was used. Figure 3.8 illustrates the differences between each variation of the liner tops for this series of tests.

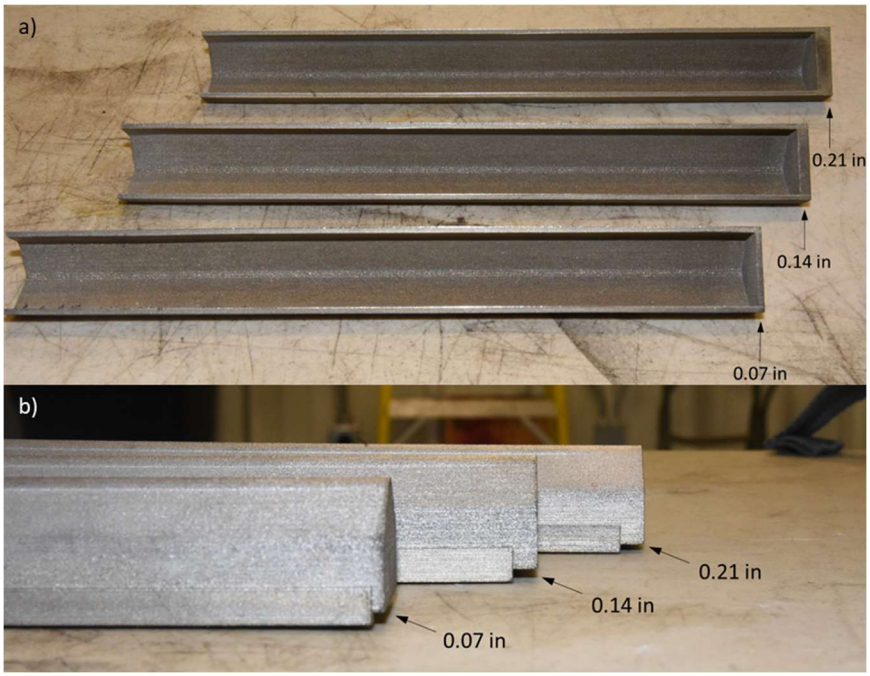

Figure 3.8 Comparison between three variations of backstops. a) Underside view of LSC liner tops. b) Side view of LSC liner with tops and bases.

Other than the backstops, the thickness of the liner remained constant throughout the entirety of the LSCs at 0.7 inches. A Renishaw AM250 selective laser melting system was used to manufacture the LSC liners with 304L stainless steel powder, and the consistency of the printed liners was 99% density bulk 304L.

Composition C-4 was hand-packed into the top liner of each LSC and molded to fit with the base liner. A mass of 89.31 grams was used to achieve a target average density of 1.6 g/cm^3 of C4, which would give a comparable amount of explosive to the referenced 1200-grain/foot copper LSC. Two hose clamps were secured on each end of each LSC to hold the charge together as seen in Figure 3.9 and Figure 3.10. Each LSC was initiated with a standard #8 electric detonator connected to an 8g pentolite cast booster to deliver a strong, consistent detonation wave to initiate the LSC. A standoff of ¾ inches was used between the LSCs and a 1 ½ inch mild steel target plate.

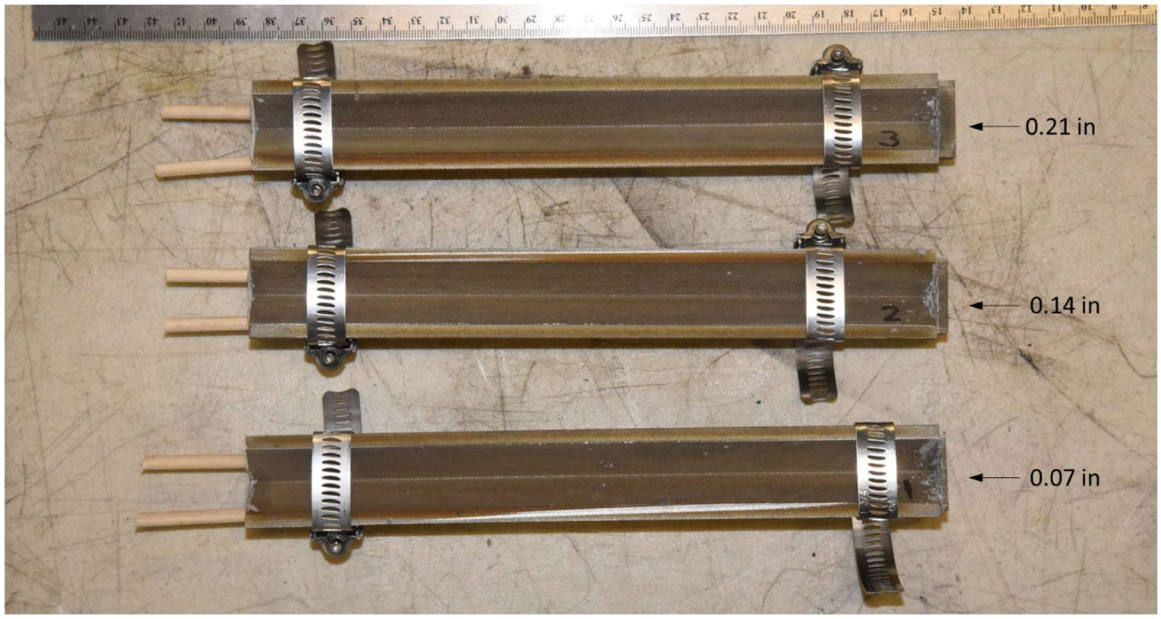

Figure 3.9 Underside view of LSCs with varying backstops.

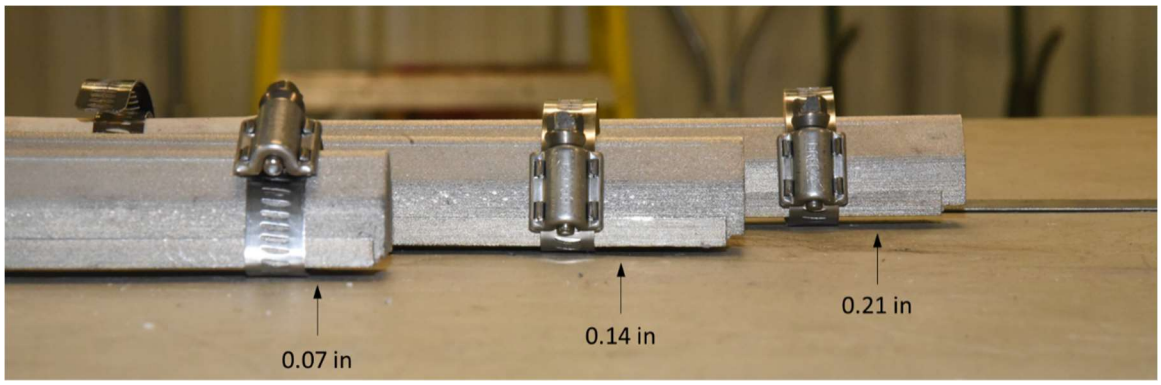

Figure 3.10 Side view of LSCs with varying backstops.

Three tests were conducted, one for each of the different backstops. Each of the resulting steel targets were washed, sliced in half down the middle of the cut made by the LSC with a water jet, lightly buffed, and coated with a thin layer of clear acrylic paint to prevent further rust build up. Table 3.3 lists the parameters of each liner that was tested for this experiment.

Table 3.3 Testing Parameters of Run down Experiment. *Volumes of LSC were calculated within Solidworks.

Test	Mass of C4 (g)	Volume of LSC (cm^3)*	Density of C4 (g/cm^3)	Backstop Thickness (in)
1	89.25	55.82	1.599	0.07
2	89.20	55.82	1.598	0.14
3	89.30	55.82	1.600	0.21

3.4. TESTING REPEATABILITY

An overall testing scheme was designed to test the repeatability of the best results from Sections 3.2 and 3.3. The parameters considered when designing this test were the

deepest average penetration that resulted in a reduction of the run up based on the results from Section 3.2, and the highest reduction of the run down area based on the results from Section 3.3. The design and testing from these experiments will be further discussed in Section 4.3.

4. RESULTS AND ANALYSIS

Run up and run down are phenomena that regularly occur with the use of linear shaped charges (LSCs). Section 4.1 will focus on the run up phenomena and the results directly associated with it. The run down testing results will be covered in Section 4.2. Section 4.3 will analyze the results of combining the parameters that gave the best performances from the run up and run down testing, while also testing the repeatability of the results from Sections 4.1 and 4.2.

4.1. RUN UP

Run up refers to the area in the initial stages of the target where the depth of penetration is constantly increasing until it reaches the steady state penetration depth and stabilizes. Run up is primarily due to the shock front propagating radially away from the point of initiation. The shock front rapidly flattens out into a planar wave as it travels through the LSC, at which point maximum penetration is achieved and the depth of penetration stabilizes [14]. However, because the shock front does not instantly become a planar wave after initiation, but rather takes a small amount of time to become one, the run up region is the result of the shock front not being fully planar yet. Based on data acquired through testing done by Nolan, et al. [20], and Ortel [21], the run up effect occurs in the initial third of the length of the LSC.

Three tests were conducted, one each for the 85°, 70°, and 55° apex angle LSCs. Each of the resulting steel targets, as shown in Figure 4.1, were washed, sliced in half

down the middle of the cut made by the LSC with a water jet, lightly buffed, and coated with a thin layer of clear acrylic paint to prevent rust build up.

Figure 4.1 Steel target results post-blast from 55° LSC.

Images of the face-cut were taken with the penetration by the LSC centered to reduce the effect of barrel distortion [41]. Images were then uploaded to OMAX LAYOUT to scale and analyze. The depth of penetration was hand-traced in LAYOUT for each target (Figure 4.2). Please refer to Appendix A for further information regarding OMAX LAYOUT and how it was used in the analysis of the results. Of note, some residue from the steel blade was left over from the LSC cut and had fused with the steel target, as shown in Figure 4.3. The residue was easy to identify as it was a lighter color than the steel target itself and was considered when tracing the depth penetration of the target.

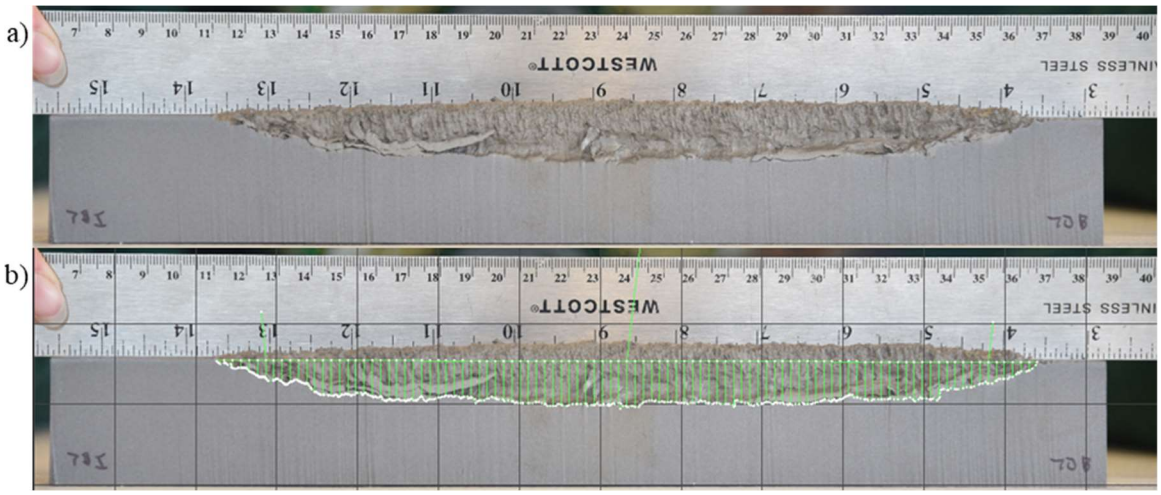

Figure 4.2 Image analysis of penetration depth. a) Image of 70° LSC target. b) Image of 70° LSC target with depth measurement overlay through OMAX LAYOUT.

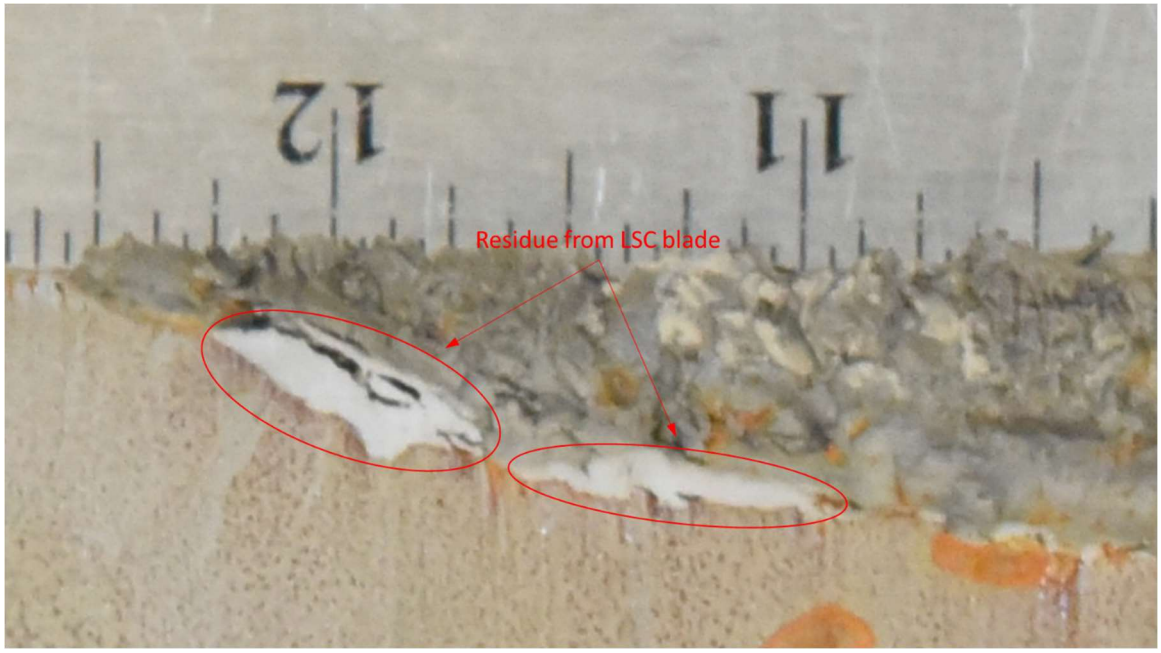

Figure 4.3 Close-up of residue left over from the LSC blade.

The analysis parameters were based off the 85° apex angle LSC results as this experimental design mimicked the dimensions of a commercial LSC and its results would

serve as the baseline control for all subsequent testing using 304L stainless steel and C4. The run up and run down "zones" were determined by taking 90 percent of the average depth penetration to create an initial reference zone to work with. Any penetration depth within 10% of the overall average depth penetration would be considered a part of the "stable cut" zone and any penetration depth outside of the 10% zone would be considered either run up or run down, depending on whether the area fell towards the initiation end or the exit end. The end points didn't have any penetration and therefore were not included in any of the penetration calculations as they had values of "0". Figure 4.4 illustrates this concept below.

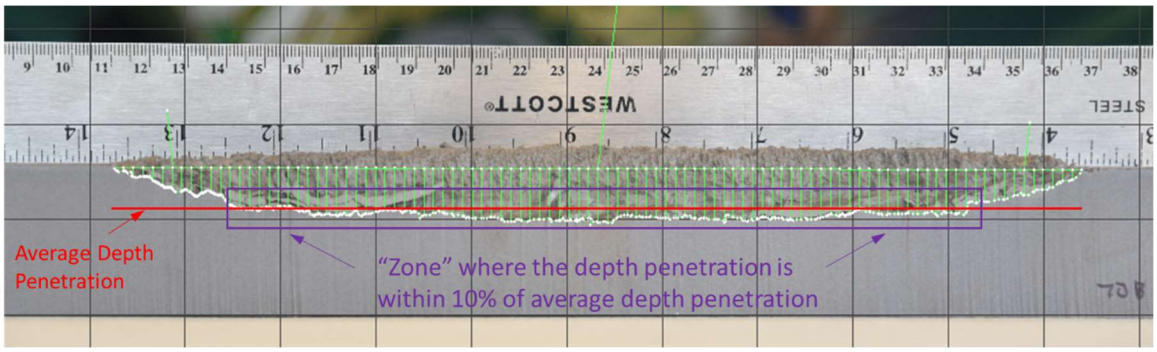

Figure 4.4 Initial step in determining the "stable cut" zone. The red line illustrates the average depth penetration of the overall cut. The purple box illustrates the data points that fall within 10% of the overall average depth penetration.

A new average was taken from all the data points that fell within the "zone" to produce a value that is more accurate to the penetration depth at which the shock front became planar and stabilized the cut. The standard deviation was calculated on this set of data points within the "zone" to determine how close together the penetration depth was

throughout this data set. The standard deviation was found to be within 7% of the "zone's" average depth penetration. Figure 4.5 depicts the overall average depth penetration and the initial zone setup as dotted lines and boxes while the average depth penetration and the zone of the "stable cut" is shown as solid lines and boxes.

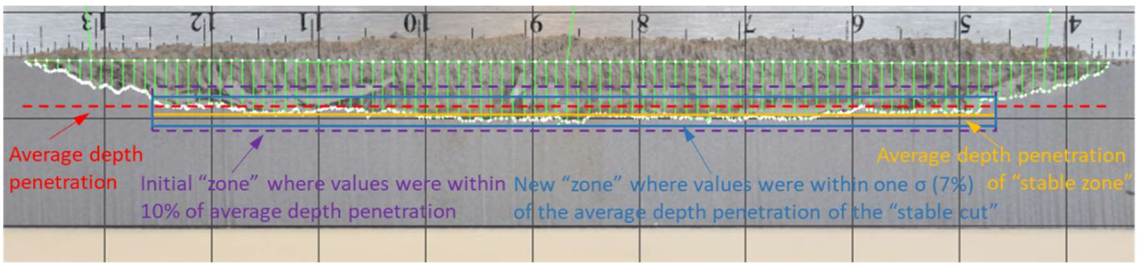

Figure 4.5 Refining the average depth penetration of the "stable zone" through standard deviation. The dotted lines and boxes depict the initial average and zone created from Figure 4.4. The solid lines and boxes depict the "stable" average depth penetration and zone.

Based on the newly found average depth penetration of the "stable cut", any data point that fell within one standard deviation, or 7%, of the average was considered to be part of the stabilized cut. Likewise, any data point that fell outside of one standard deviation was considered either run up or run down, depending on whether the area was towards the initiating end or the exit end. Figure 4.6 below illustrates these newly defined areas.

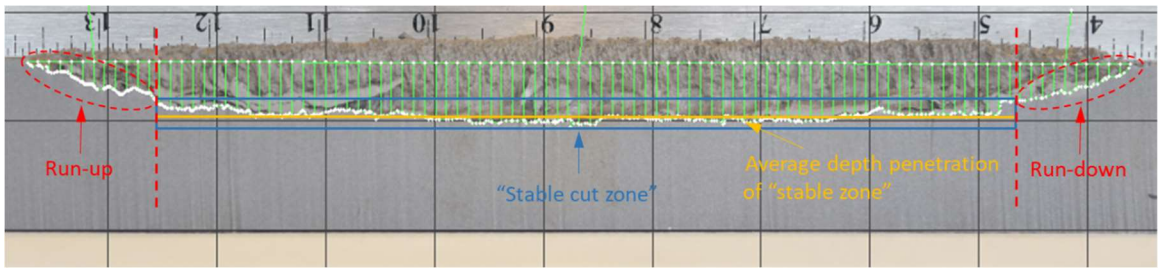

Figure 4.6 Defining the run up and run down areas of the cut.

This initial analysis was performed on the 85° LSC which had the exact same dimensions as the commercially available 1200 gr/ft copper LSC. This analysis was therefore treated as the control of all testing performed, and the 7% deviation from the average depth penetration of the "stable zone" was used as the standard for all subsequent analysis.

The results of the penetration depth tests are listed in Table 4.1. The overall length of penetration into the steel target was greater than the length of the LSC (9 inches). This may be due to an increase in confinement because the liner is made of steel rather than copper or focused spalling from the lateral at these areas.

Table 4.1 Results of Penetration Depth Tests

Test	Density of C4 (g/cm^3)	% of Cut Length that is Run up	Actual Run Up Length (in)	Maximum Depth Penetration (in)	Average Depth of Penetration w/o Run up/Run down (in)
85° apex angle LSC (Control)	1.600	11.00%	0.33	0.54	0.47
70° apex angle LSC	1.601	11.00%	0.39	0.57	0.49
55° apex angle LSC	1.599	10.00%	0.38	0.62	0.55

The percentage of cut length that is run up was much lower than initially expected. This is most likely due to Nolan, et al. [20], and Ortel's [21] data resulting from a 10,500 grain per foot LSC. The size and dimensions of the 10,500 grain per foot LSC coupled with the initiation method and placement may have contributed to the overtly large run up area and explain why the percentage of run up did not scale with size.

The percentage of run up is slightly reduced as the apex angle becomes more acute, which indicates the change in apex angle may affect the amount of run up that occurs, but not definitively enough to enact a noticeable change. The initial test results did not indicate an effect of apex angle on the amount of run up that occurs, so repeatability testing was not conducted for any angles from test series 1.

The maximum depth penetration as well as the average penetration of the stable cut zone was higher for the more acute apex angle LSCs. It is interesting to note that even though all of the LSCs returned to an 85° apex angle after the initial 3 inches, the increase in average depth penetration remained consistent. If the initial 3 inches of the cut are excluded to account for any variance that may be due to differing apex angles, there is an increase of 19% in average depth penetration between the cuts made by the portions of the 85° LSC and the 55° LSC that have the same apex angle.

4.2. RUN DOWN

In a similar vein to run up, run down refers to the area in the latter stages of the target where the depth of penetration decreases. Run down may be due to a lack of confinement at the exit end of the LSC in which much of the energy disperses out the unconfined end of the liner rather than towards forming the blade. It may also be due to

running out of explosive material to continue to propagate the shock front, as longer LSCs only display the run down effect at the very end. In other words, the planar shock front would continue on indefinitely, as long as there was a continuous feed of explosive material to propagate the detonation.

The results from the experiments performed in Section 3.4 are analyzed below. Images of the cut were taken with the penetration centered and at maximum zoom to reduce the effect of barrel distortion. Images were then uploaded on OMAX LAYOUT to scale and analyze. The depth of penetration was hand-traced in LAYOUT for each target, same as described in Section 4.1.

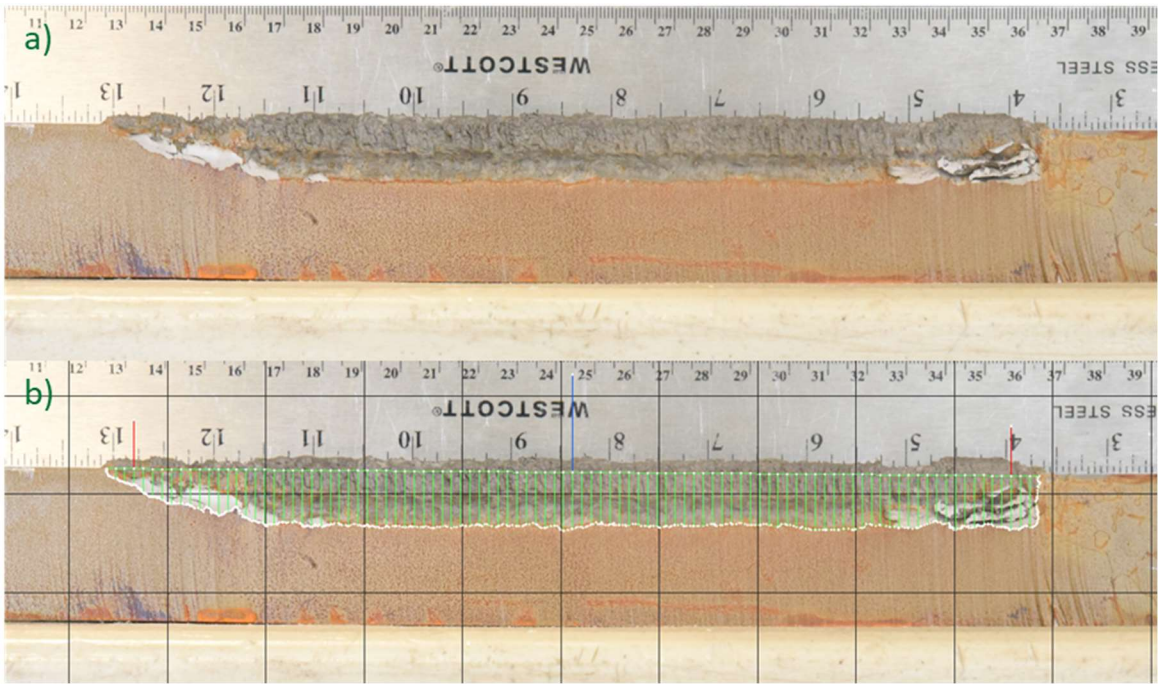

Figure 4.7 Image analysis of penetration depth. a) Image of 0.21-in. backstop target. b) Image of 0.21-in. backstop target with depth measurement overlay through OMAX LAYOUT.

A side by side comparison between images of the results from the “Run up” test series to the results from the “Run down” test series illustrate the drastic difference in run down that occurred, as seen in Figure 4.8. The “Run up” test series has a gradual incline towards the right side, indicative of the run down region caused by the LSC. This sharply contrasts with the run down region in the “Run down” test series, which maintains the overall depth penetration of the cut until the end where the cut ends at ~90° angle. Both images are the results of a consistent 85° apex angle base; the only difference between the two LSC charges was the implementation of a backstop for the “Run down” test series. The backstop implemented with the LSC tops has effectively reduced the run down region of the cuts to less than 1%.

Figure 4.8 Comparison of “Run up” and “Run down” test results. a) Results from 85° apex angle LSC, “Run up” test series. b) Results from 0.14 inch backstop LSC, “Run down” test series.

The results of the depth of penetration tests are listed in Table 4.2. The run down phenomena still exists at a reduced rate with the 0.07 inch backstop, but is completely

eliminated with the 0.14 inch and 0.21 inch backstops. The run up and run down zones were determined based on the control set of 7% within the average overall penetration, as explained in Section 4.1.

Table 4.2 Results of Depth of Penetration Tests

Test	Density of C4 (g/cm^3)	% of Cut Length that is Run down	Maximum Depth Penetration (in)	Average Depth of Penetration w/o Run up (in)
85° apex angle LSC (Control)	1.600	17.00%	0.54	0.47
0.07 inch backstop	1.599	1.01%	0.64	0.57
0.14 inch backstop	1.598	0%	0.63	0.56
0.21 inch backstop	1.600	0%	0.60	0.54

4.3. COMBINING RUN UP AND RUN DOWN RESULTS TO TEST CONSISTENCY OF RESULTS

A new series of tests were developed and conducted to evaluate the consistency of the results obtained from the previous run up and run down testing and to determine if the two separate LSC designs would complement each other. The LSC designs that had the best performance towards reducing run up and run down were tested. This meant combining the 55° extruded LSC base with the 0.14-inch thick backstop LSC top as shown in Figure 4.9. Results from the previous test indicated that the 0.14-inch and the 0.21-inch backstops both reduced the amount of run down to 0% remaining. Based on

results from previous testing done, a 0.14-inch backstop was implemented for final testing.

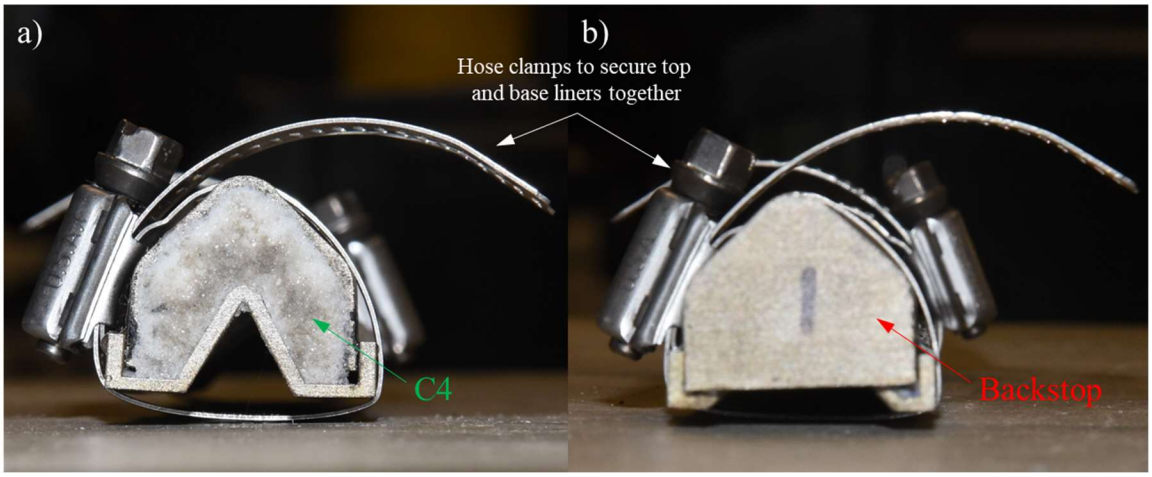

Figure 4.9 Close-up view of packed LSC charge. a) View of initiation end of LSC. b) View of exit end of LSC with 0.14-inch backstop.

Other than the backstops, the thickness of the liner remained constant throughout the entire length of the LSCs at 0.7 inches. A Renishaw AM250 selective laser melting system was used to manufacture the LSC liners with 304L stainless steel powder, and the consistency of the printed liners was 99% density bulk 304L to stay consistent with previous testing.

Composition C-4 was hand-packed into the top liner of each LSC and molded to fit with the base liner. A target mass of 91.76 grams was used to achieve an average density of 1.6 g/cm^3 of C4, which would give a comparable amount of explosive to the referenced 1200-grain/foot copper LSC. A hose clamp was secured on both ends of each LSC to hold the charge together. The complete ensemble of LSC charges to be tested are

shown in Figure 4.10. Each LSC was initiated with a standard #8 electric detonator connected to an 8g pentolite cast booster to deliver a strong, consistent detonation wave to initiate the LSC. A standoff of ¾ inches was used between the LSCs and a 1 ½ inch mild steel target plate, based on published recommended standoff values [39]. An example of the initial setup is shown in Figure 4.11 and Figure 4.12 displays the test setup just prior to initiation.

Figure 4.10 Topside view of LSCs. Wooden dowels are attached to help anchor the 8g cast boosters to the LSC charges.

Figure 4.11 Side view of test setup with ¾" standoffs.

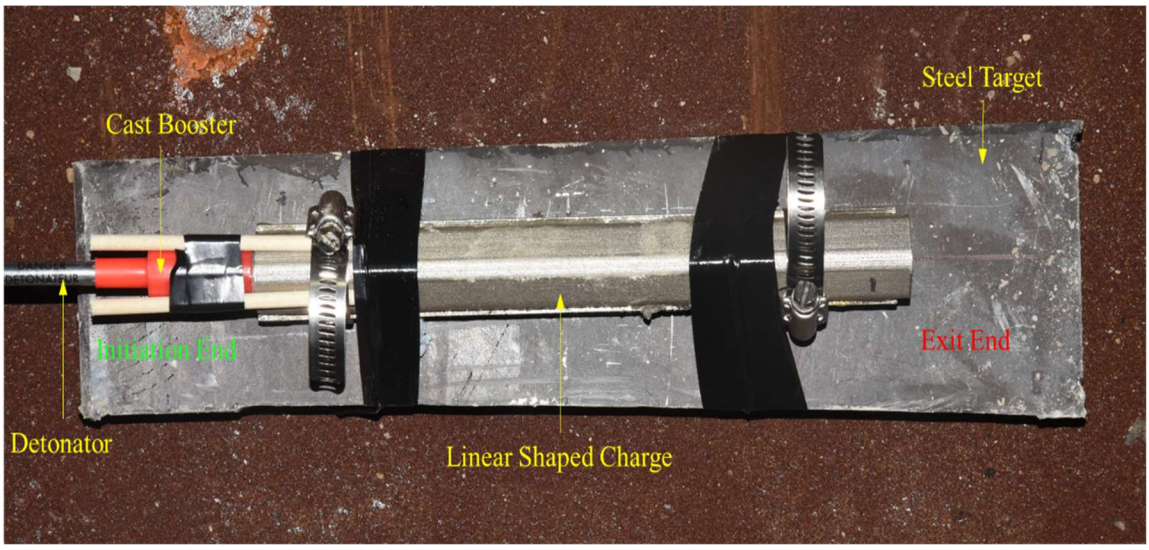

Figure 4.12 Topside view of final test setup prior to initiation.

Five tests were conducted in total, each test with the same charge and liner dimensions and materials. Each of the resulting steel targets were washed, sliced in half down the middle of the cut made by the LSC with a water jet, lightly buffed, and coated with a thin layer of clear acrylic paint to prevent rust build up. Images of the cut were taken with the penetration centered and at maximum zoom to reduce the effect of barrel distortion. Images were then uploaded on OMAX LAYOUT to scale and analyze as shown in Figure 4.13. The depth of penetration was hand-traced in LAYOUT for each target, same as with the previous test series results.

The results of the depth penetration tests are listed in Table 4.3. The run up and run down areas were determined based on the control set of 7% within the average overall penetration, as explained in Section 4.1.

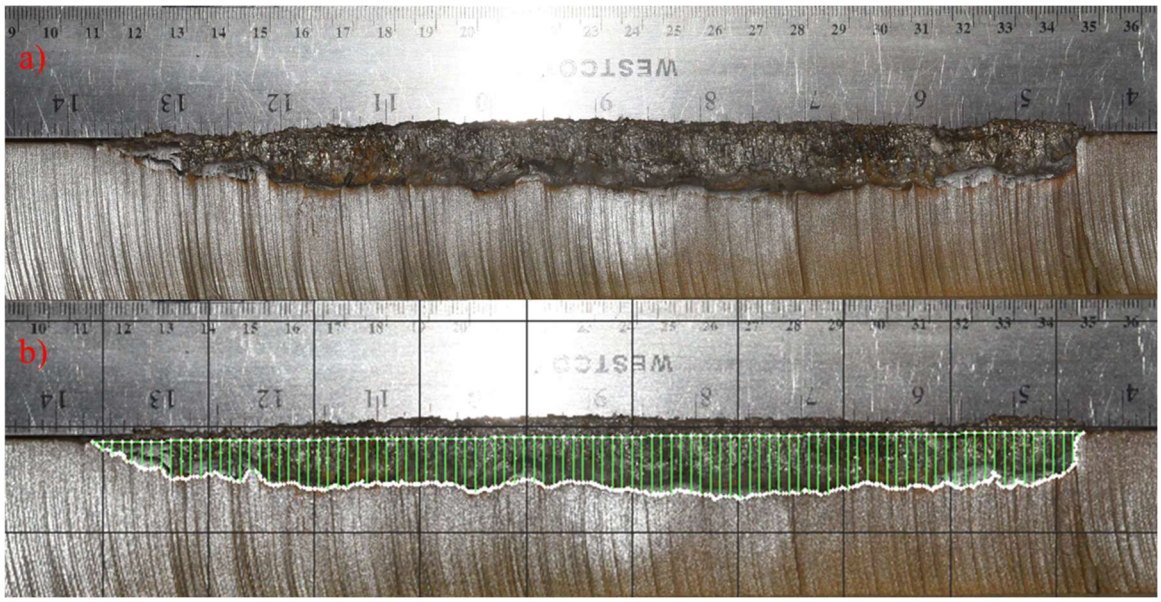

Figure 4.13 Image analysis of penetration depth. a) Image of #3 test result. b) Image of same #3 test result but with depth measurement overlay through OMAX LAYOUT.

Table 4.3 Results of Depth Penetration Tests

Test	Density of C4 (g/cm^3)	% of Cut Length that is Run up	Actual Run up Length (in)	% of Cut Length that is Run down	Maximum Depth Penetration (in)	Average Depth of Penetration w/o Run up/Run down (in)
85° apex angle LSC (Control)	1.600	11.00%	0.33	17.00%	0.54	0.47
#1	1.601	14.00%	0.39	2.00%	0.60	0.53
#2	1.599	17.00%	0.44	1.00%	0.62	0.54
#3	1.598	18.00%	0.41	1.00%	0.59	0.48
#4	1.599	19.00%	0.36	0.00%	0.50	0.52
#5	1.600	17.00%	0.36	1.00%	0.61	0.51
Average	1.599	17.00%	0.39	1.00%	0.60	0.52

In all five tests, run up averaged 17% of the cut and run down consistently averaged 1% of the cut. While the percentage of run up at first glance seems to be larger for the third series tests, upon looking closer at the actual data reveals that the actual

length of run up is very similar to the control result. The main reason why the percentage of run up seems larger is because the entire cut length is, on average, half an inch shorter than the control cut length. The maximum depth of penetration between the tests was within 0.025 inches of each other, while the average depth of penetration were within 0.0625 inches of each other. The results show the overall depth penetration to be consistent within the test series.

The standard deviations of average depth penetration, average depth penetration without run up/run down, and the percentage standard deviation is of the average depth penetration run up/rundown are all fairly similar to each other across all five tests as well. This further validates the consistency of the results. Table 4.4 compares the standard deviations of the results of the depth penetration tests.

Table 4.4 Standard Deviation Results of Depth Penetration Tests

Test	Standard Deviation of Average Depth Penetration (in.)	Standard Deviation of Average Depth Penetration without Run up/Run down (in.)	% a STD is from Average Depth Penetration without Run up/Run down
#1	0.12	0.04	7%
#2	0.12	0.05	8%
#3	0.10	0.06	12%
#4	0.11	0.04	8%
#5	0.12	0.06	12%

The results also show the maximum depth penetration as well as the average depth penetration without run up/run down to be higher in every test compared to the results of the 85° apex angle LSC from Section 4.1. The average between the five tests for average depth penetration without run up/run down calculates out to 0.52 inches

penetration compared to the 85° LSC result of 0.47 inches. The average maximum depth penetration between the five tests is 0.60 inches compared to the 85° LSC result of 0.54 inches.

5. CONCLUSIONS

Run up and run down are regularly occurring phenomena resulting from the use of linear shaped charges. While commercial uses have implemented work arounds for the run up and run down phenomena, such as using longer lengths of linear shaped charges to ensure the targeted cut zone does not fall within the range of the run up and run down zones, there may be certain situations that arise in which greater precision is required, such as cutting with curved LSCs. This research was intended to explore possible methods of reducing the amount of run up and run down that occurs by altering the structural composition of a conventional linear shaped charge through the use of additive manufacturing while also confirming the applicability of using AM techniques for shaped charges. Two experimental test series were developed for testing the following hypotheses:

- 1) Adjusting the initial apex angle of a linear shaped charge liner reduces the amount of run up that occurs.
- 2) Implementing a backstop at the end of a linear shaped charge liner reduces the amount of run down that occurs.

The results from testing hypothesis 1) show that changing the apex angle did not yield a large amount of reduction in run up area. The difference in percentage of run up as part of the overall cut length was 1% less between a LSC with an apex angle of 55° to a LSC with an apex angle of 85°. There was no difference in percentage of run up as part of the overall cut length between a LSC with an apex angle of 70° to a LSC with an apex angle of 85°. However, the results also showed that changing the apex angle did yield a

higher maximum and average penetration depth in the overall cut. Further testing can be done in the future to determine why this happened and whether is it commercially viable.

The results from testing hypothesis 2) show that implementing a backstop greatly reduced the amount of run down. Run down was reduced to 1% of the overall cut length over all three trials of different thickness backstops. Therefore, it can be concluded that the implementation of a backstop successfully all but eliminates the run down that occurs through conventional linear shaped charge use by containing energy within the cut length and directing it into blade formation and penetration. This is deemed a novel use of additive manufacturing to improve the performance of LSCs with the potential for industry implementation and use.

A third experimental test series was designed to combine the continuously changing apex angle along with the implementation of a backstop. The intent of this experimental test series was twofold: first, to see if both changes could work together and still function as a linear shaped charge. Second, to test the repeatability of the first two testing series and see if similar results could be reproduced. Although changes in run up using the 55° angle in test series one did not yield significant changes over the straight design, it was decided to repeat this design change and further investigate the run up phenomena. The repeatability tested for this one series is indicative of precision and repeatability in the overall results. The run up percentages were within five percentage points of each other and the run down percentages were within two percentage points of each other, within this third test series. And when comparing the actual length of the run up between the results from the third test series and the control results, the results are very similar to each other; a run up length of 0.33 inches for the control, and an average

run up length of 0.36 inches for the third test series. The results of the third experimental test series appears to correlate testing for significance as a future work. The average and maximum penetration depths from the third experimental test series were also similar to their corresponding values from the first and second test series.

The use of additive manufacturing was successful in creating working prototypes of linear shaped charge liners, capable of achieving similar results to conventionally-made linear shaped charge liners. An advantage seen with additive manufacturing was the ease of creating a custom liner and making several small adjustments to the liner throughout the course of testing.

APPENDIX A

OMAX LAYOUT PRIMER

The purpose of this primer is to illustrate how the CAD software, OMAX LAYOUT Premium, was utilized to measure and analyze the penetration depth into the steel targets made by the custom LSCs.

The software, OMAX LAYOUT Premium, must be opened first. This can be done either via shortcut or through the Start menu. Once the program is running, load the image to be measured and analyzed by locating “Image Tracing” from the top dropdown menu and selecting the “Load Image for Tracing…” option as shown in Figure A.1.

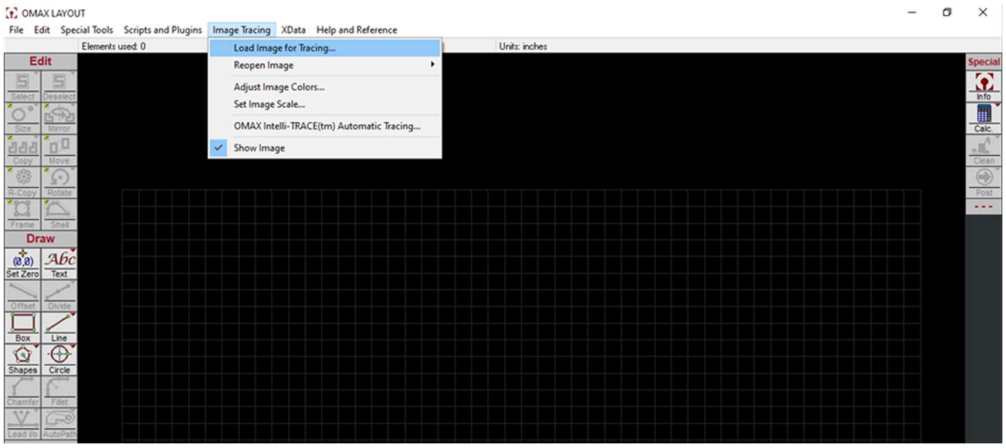

Figure A.1 Load image for tracing in OMAX LAYOUT

Once the image has loaded into the program, the scale must be set in order to normalize the dimensions from the photo with the dimensions in the program. First, measure out a line according to the scale present within the image. As the example in Figure A.2 shows, a line is created between the eighth and ninth inch markings of the ruler present in the image. Further inspection reveals the line to be 4.55 inches long to the one inch scale in the image, or a ratio of 4.55 to 1.

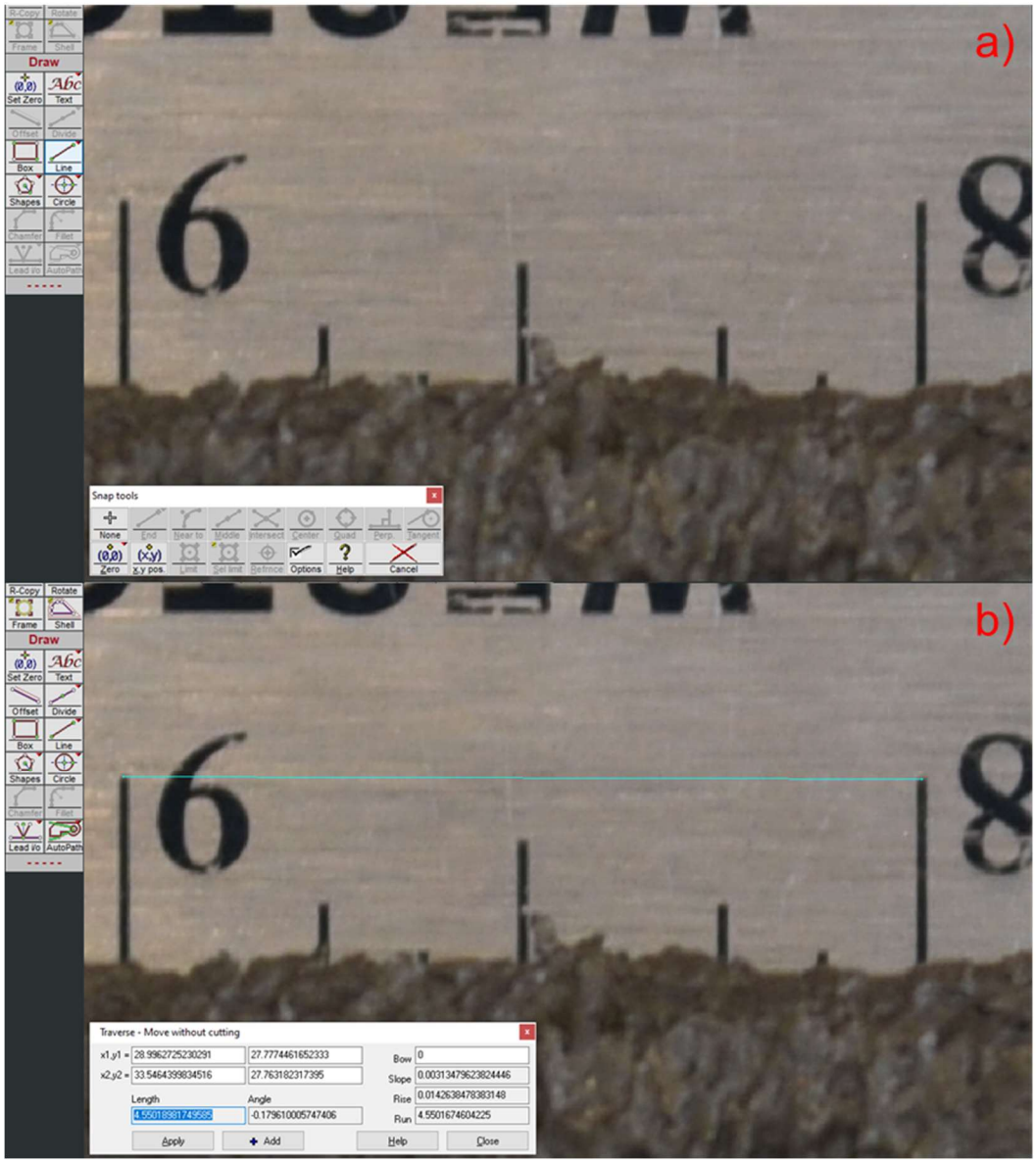

Figure A.2 Normalizing scale of image in program. a) 8 and 9 inch markings chosen as reference point. b) Ratio of scale is 4.55:1.

After the readjustment of the image size in the program such that one inch in the program equals one inch on the image, measurement of the cut can begin. A line is drawn across the top surface of the target to denote the null penetration level as shown in Figure A.3. Then the “Continuous line” function is used to start tracing out the cut in the target.

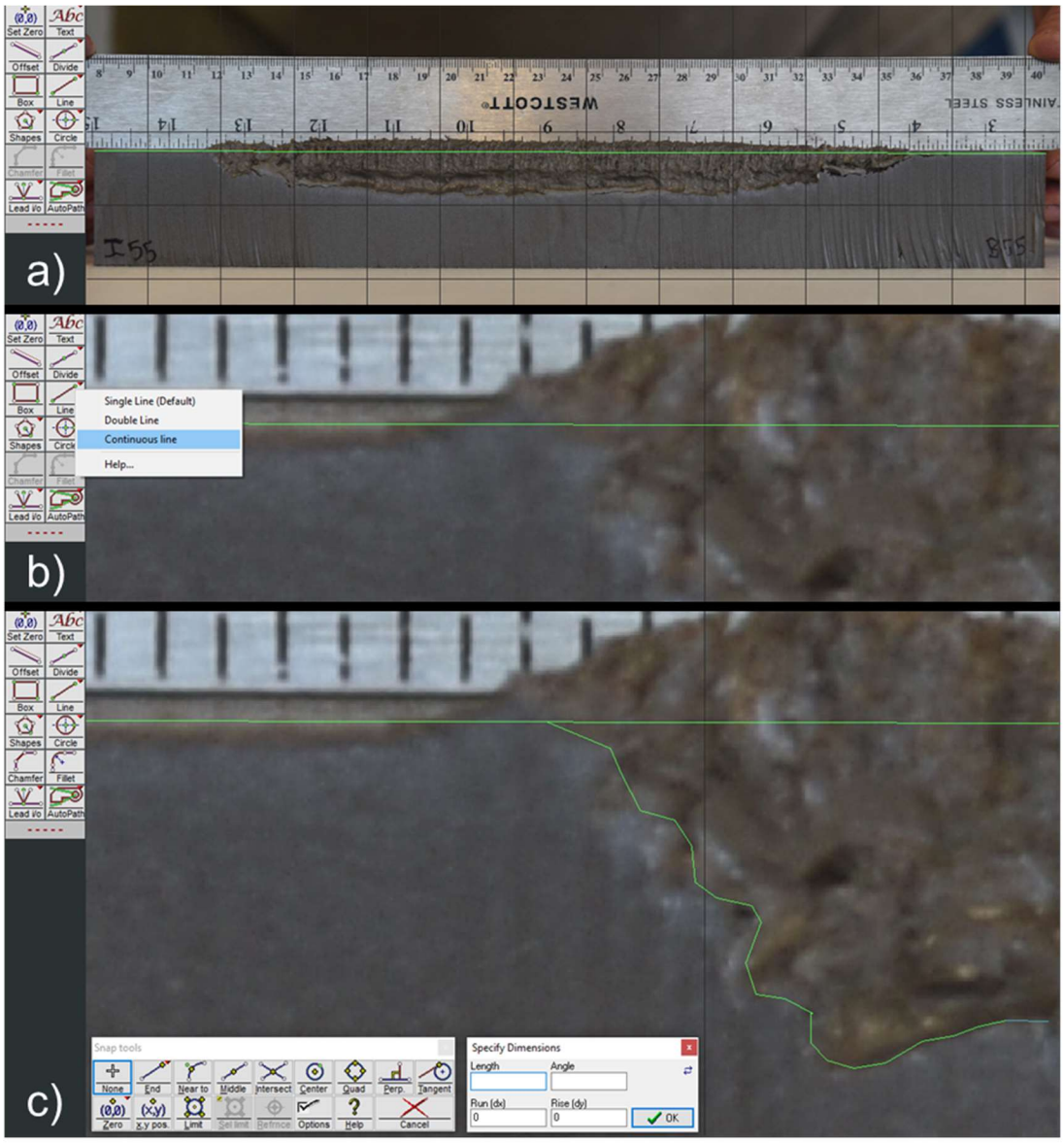

Figure A.3 Tracing the cut. a) Setting the null penetration line. b) Selecting the "Continuous line" function. c) Tracing the cut.

Once the entire cut is traced, the null penetration line is divided into 100 equal sections to use as data points. This is done by selecting the line (highlighted in yellow) and selecting the "Divide into equal sections" function, and then inputting the desired number of segments as shown in Figure A.4.

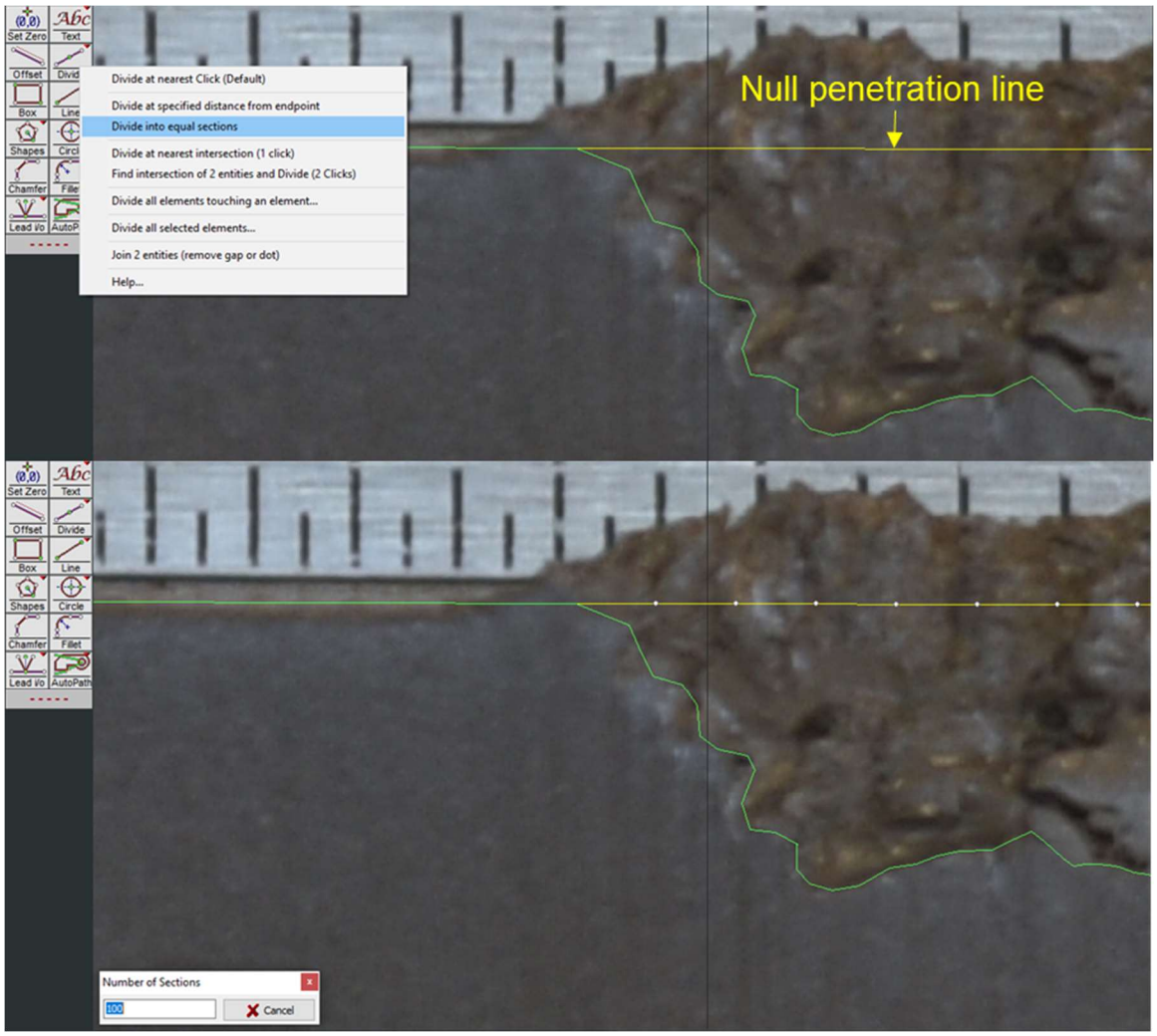

Figure A.4 Dividing null penetration line into segments.

Lines are now drawn originating from each node along the null penetration line and extended past the tracing of the cut. This process is expedited using the “Copy” function. All of the new lines are drawn perpendicular to the null penetration line as shown in Figure A.5.

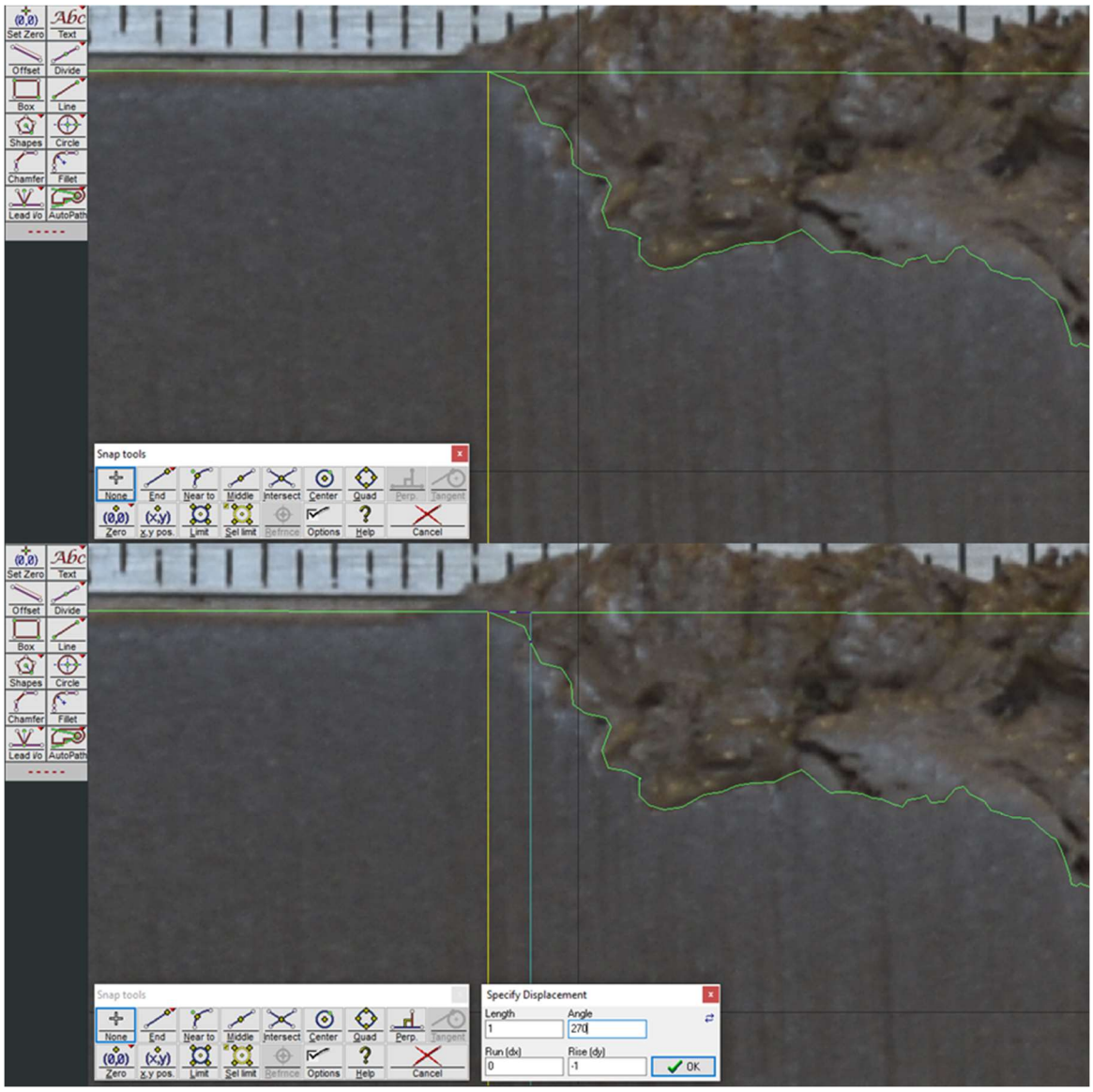

Figure A.5 Drawing lines extending past the tracing and perpendicular to the null penetration line.

The last step required is to separate the lines that extend past the tracing from the tracing itself. This is done with the “Divide at the nearest intersection” function by manually clicking on each perpendicular line at the spot where it intersects the tracing.

Once all extraneous lines are disconnected, selecting them and deleting them will tidy up the image as shown in Figure A.6.

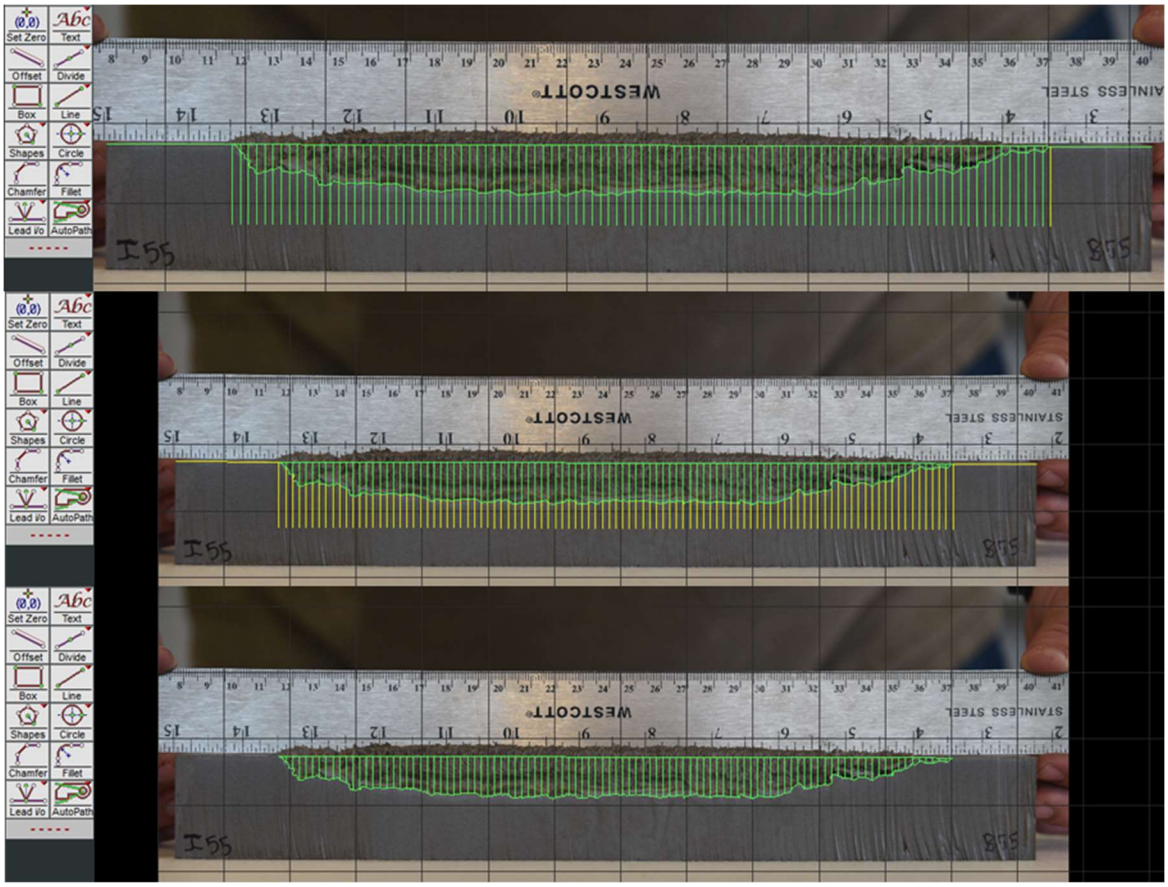

Figure A.6 Deletion of all extraneous lines.

Measurements can now be taken by using the measuring tool and highlighting each individual line to bring up its information. The length of each line directly corresponds to the penetration depth of that line.

APPENDIX B

CACHE OF IMAGES USED FOR ANALYSIS

The following images were used to analyze the penetration of the cut into steel targets. Images included are ordered as follows:

1) Test Series 1: 85° Apex Angle (Control), 70° Apex Angle, 55° Apex Angle.
2) Test Series 2: 0.07 inch backstop, 0.14 inch backstop, 0.21 inch backstop.
3) Test Series 3: Trial #1, Trial #2, Trial #3, Trial #4, Trial #5.

Figure B.1 Image of Test Series 1: 85° Apex Angle (Control)

Figure B.2 Image of Test Series 1: 70° Apex Angle

Figure B.3 Image of Test Series 1: 55° Apex Angle

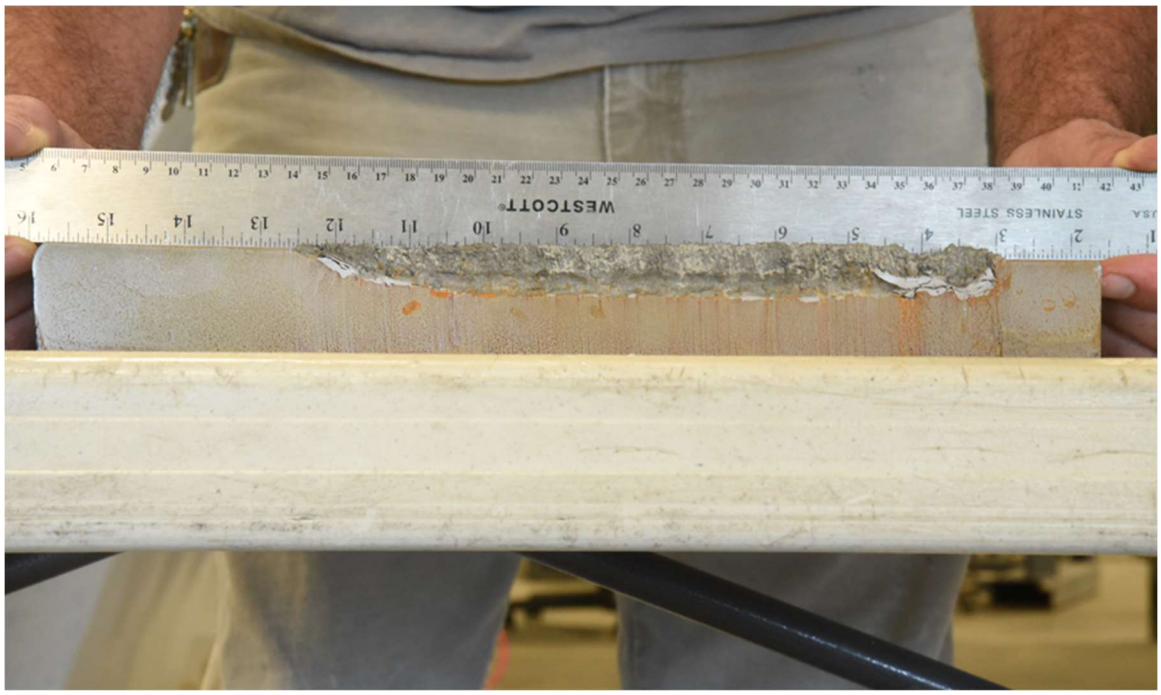

Figure B.4 Test Series 2: 0.07 inch backstop

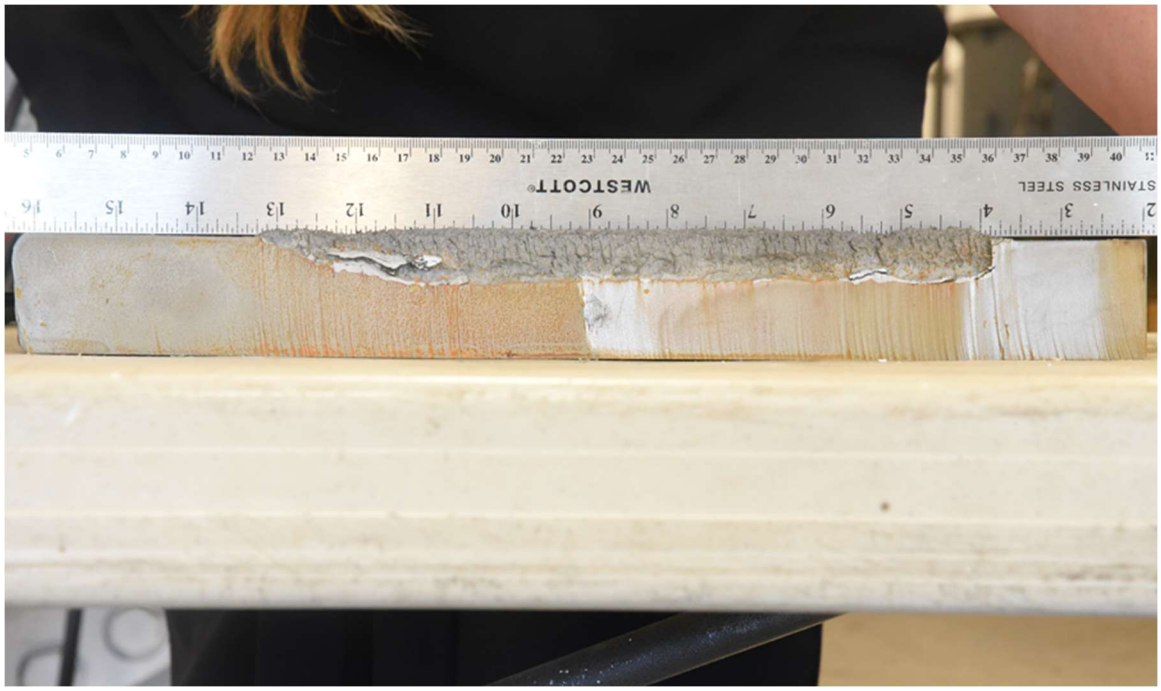

Figure B.5 Test Series 2: 0.14 inch back stop

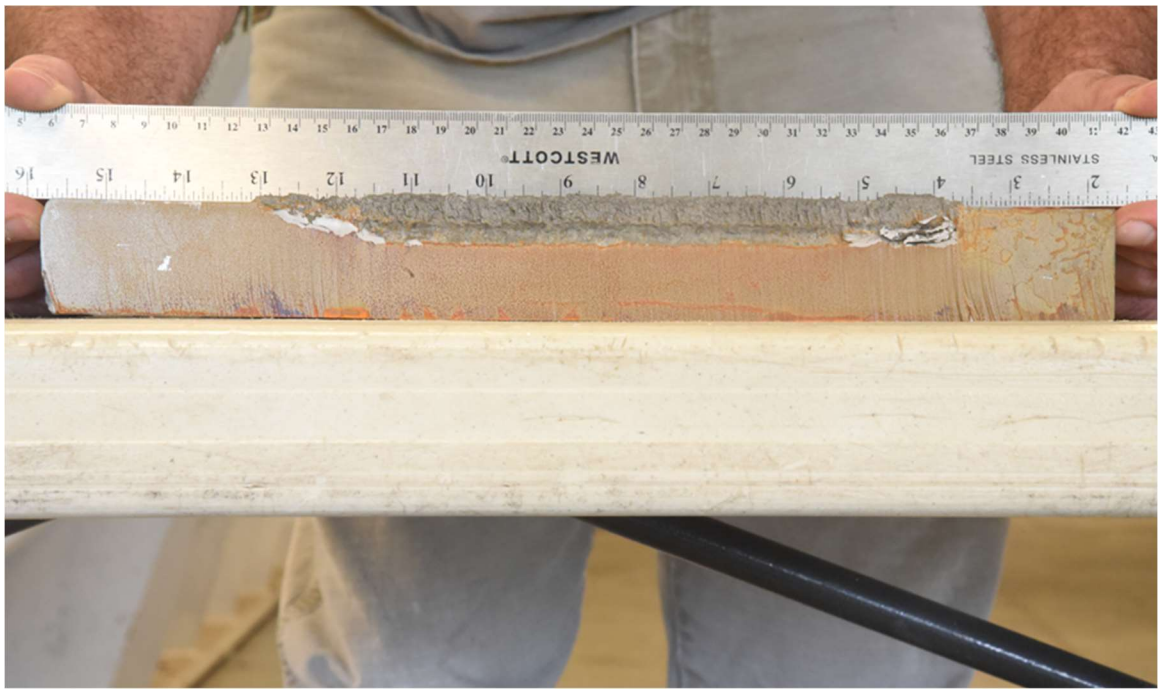

Figure B.6 Test Series 2: 0.21 inch backstop

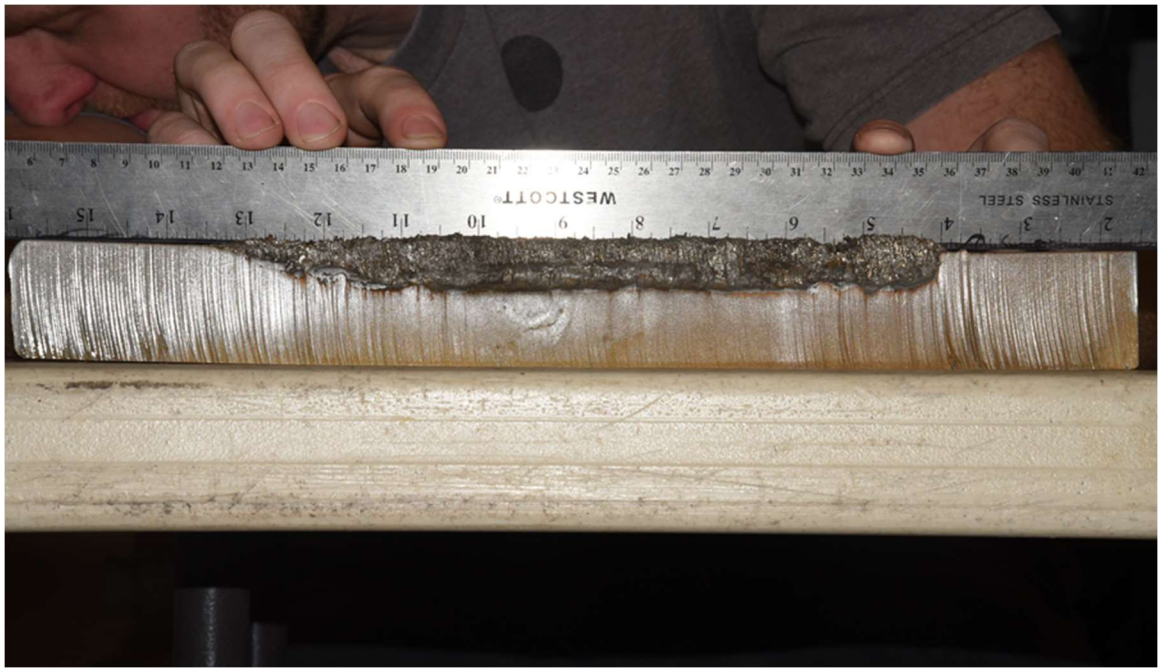

Figure B.7 Test Series 3: Trial #1

Figure B.8 Test Series 3: Trial #2

Figure B.9 Test Series 3: Trial #3

Figure B.10 Test Series 3: Trial #4

Figure B.11 Test Series 3: Trial #5

REFERENCES

[1] W. P. Walters and J. A. Zukas, Fundamentals of Shaped Charges, Baltimore: CMCPress, 1998.

[2] K. Phelps, Interviewee, *Phone conversation.* [Interview]. 15 April 2019.

[3] D. Novotney and M. Mallery, "Historical Development of Linear Shaped Charge," in *43rd AIAA/ASME/SAE/ASEE Joint Propulsion Conference & Exhibit*, Cinicinnati, 2007.

[4] W. Walters, "A Brief History of Shaped Charges," in *24th International Symposium on Ballistics*, New Orleans, LA, 2008.

[5] P. W. Cooper, Explosives Engineering, New York: Wiley-VCH, 1996.

[6] G. Birkhoff, D. P. MacDougall, E. M. Pugh and S. G. Taylor, "Explosives with Lined Cavities," *Journal of Applied Physics,* vol. 19, pp. 563-582, 1948.

[7] M. G. Vigil, "Optimized Conical Shaped Charge Design Using the SCAP Code," Sandia National Labs, Albuquerque, New Mexico, 1988.

[8] G. A. Hayes, "Linear shaped-charge (LSC) collapse model," *Journal of Materials Science,* pp. 3049-3058, 1984.

[9] PacSci EMC, "Linear Shaped Charge," November 2019. [Online]. Available: https://psemc.com/products/linear-shaped-charge/.

[10] E. L. Baker, W. J. Poulos, S. E. DeFisher, T. M. Madsen, J. M. Pincay, A. D. Wilson, B. E. Fuchs and A. S. Daniels, "Water as a Linear Shapped Charge Liner Material," in *27th International Symposium on Ballistics*, Freiburg, 2013.

[11] D. R. Kennedy, "History of the Shaped Charge Effect, The First 100 Years," in *100th Anniversary of the Discovery of the Shaped Charge Effect*, West Germany, 1983.

[12] J. A. Zukas and W. Walters, Explosive Effects and Applications, New York: Springer-Verlag, 1998.

[13] P. W. Cooper and S. R. Kurowski, Introduction to the Technology of Explosives, Wiley-VCH, 1996.

[14] S. Lim, *MS Thesis, An Investigation of the Characteristics of Linear Shaped Charges Used in Demolition,* Rolla, MO: Missouri Univeristy of Science and Technology, 2003.

[15] S. Lim, *PhD Dissertation, A Preliminary Investiagtion of the Blade Formation and Cutting Process of the Linear Shaped Charges,* Rolla, 2006.

[16] S. Lim and et al., "Mechanisms of Linear Shaped Charge Cutting - A New Explanation," in *Proceedings of the 31st Annual Conference on Explosives and Blasting Technique*, Orlando, FL, 2005.

[17] S. Lim and et al., "Mechanics of the Run Up on Linear Shaped Charges Cuttings," in *Proceedings of the Annual Conference on Explosives and Blasting Technique*, International Society of Explosives Engineers, 2006.

[18] S. Lim, "Steady state equation of motion of a linear shaped charges liner," *International Journal of Impact Engineering,* vol. 44, pp. 10-16, 2011.

[19] B. Burch, *MS Thesis, Determining and mitigating the effects of firing a linear shaped charge under water,* Rolla: Missouri University of Science and Technology, 2014.

[20] D. Nolan, K. Phelps, P. Mulligan and J. Baird, "Performance Evaluation and Effects of Standoff on 10,500 grain per foot Linear Shaped Charge," in *Proceedings of the Thirty-Ninth Conference on Explosives and Blasting Technique*, Fort Worth, 2013.

[21] O. M, *MS Thesis, A Modified Initiation and Cut Profile Study of the 10,500 grain per foot Linear Shaped Charge,* Rolla, MO: Missouri University of Science and Technology, 2014.

[22] ISO/TC 261, ASTM Committee F42, "ISO/ASTM 52900:2015(en)," 12 March 2020. [Online]. Available: https://www.iso.org/obp/ui/#iso:std:iso-astm:52900:ed-1:v1:en.

[23] I. R. D. S. B. Gibson, Additive Manufacturing Technologies, New York, NY: Springer, 2015.

[24] Voxeljet Services, "Voxeljet Applications : brochure," 16 March 2020. [Online]. Available: https://www.voxeljet.com/fileadmin/user_upload/PDFs/Servicebrochure_2018_web_01.pdf.

[25] TRUMPF Inc., "Laser metal deposition," 16 March 2020. [Online]. Available: https://www.trumpf.com/filestorage/TRUMPF_Master/Applications/Broschueres/TRUMPF-laser-metal-deposition-EN.pdf.

[26] Engineering Product Design, "Powder Bed Fusion," 17 March 2020. [Online]. Available: https://engineeringproductdesign.com/knowledge-base/powder-bed-fusion/.

[27] M. Yakout, M. Elbestawi and S. C. Veldhuis, "Density and mechanical properties in selective laser melting of Invar 36 and stainless steel 316L," *Journal of Materials Processing Tech.,* vol. 266, pp. 397-420, 2019.

[28] I. Tolosa, F. Garciandia and F. Zubiri, "Study of mechanical properties of AISI 316 stainless steel processed by "selective laser melting", following different manufacturing strategies.," *The International Journal of Advanced Manufacturing Technology,* vol. 51, pp. 639-647, 2010.

[29] S. Li, H. Hassanin, M. M. Attallah, N. J. Adkins and K. Essa, "The development of TiNi-based negative Poisson's ratio structure using selective laser melting," *Acta Materialia,* vol. 105, pp. 75-83, 2016.

[30] Q. Jia and D. Gu, "Selective laser melting additive manufacturing of Inconel 718 superalloy parts: Densification, microstructure and properties," *Journal of Alloys and Compounds,* vol. 585, pp. 713-721, 2014.

[31] A. El-Desouky, M. Carter, M. Mahmoudi, A. Elwany and S. LeBlanc, "Influences of energy density on microstructure and consolidation of selective laser melted bismuth telluride thermoelectric powder," *Journal of Manufacturing Processes,* vol. 25, pp. 411-417, 2017.

[32] B. Franco, J. Ma, B. Loveall, G. Tapia, K. Karayagiz, J. Liu, A. Elwany, R. Arroyave and I. Karaman, "A Sensory Material Approach for Reducing Variability in Additvely Manufactured Metal Parts," *Scientific Reports,* vol. 7, no. 3064, 2017.

[33] M. Elahinia, N. S. Moghaddam, M. T. Andani, A. Amerinatanzi, B. A. Bimber and R. F. Hamilton, "Fabrication of NiTi through additive manufacturing: A review," *Progress in Materials Science,* vol. 83, pp. 630-663, 2016.

[34] J. M. Walker, C. Haberland, M. T. Andani, H. E. Karaca, D. Dean and M. Elahinia, "Process development and characterization of additively manufactured nickel-titanium shape memory parts," *Journal of Intelligent Material Systems and Structures,* vol. 27, no. 19, pp. 2653-2660, 2016.

[35] RapidMade, "What's the Difference Between SLS and SLM?," RapidMade, Inc., 30 June 2014. [Online]. Available: https://www.rapidmade.com/rapidmade-blog/2014/6/30/ycjnxytvpt8n85gqutk5wj67cmx4t7. [Accessed 17 March 2020].

[36] R. Noe, "Production Methods: What's the Difference Between Selective Laser Sintering, Direct Metal Laser Sintering, Laser Melting and LaserCusing?," core77.com, 18 February 2014. [Online]. Available: https://www.core77.com/posts/26457/Production-Methods-Whats-the-Difference-Between-Selective-Laser-Sintering-Direct-Metal-Laser-Sintering-Laser-Melting-and-LaserCusing. [Accessed 17 March 2020].

[37] C. Y. Yap, C. K. Chua, Z. L. Dong, Z. H. Liu, D. Q. Zhang, L. E. Loh and S. L. Sing, "Review of selective laser melting: Materials and applications," *Applied Physics Reviews,* vol. 2(4), no. 041101-, pp. 1-21, 2015.

[38] J. Ho, C. Lough, P. Mulligan, E. Kinzel and C. Johnson, "Additive Manufacturing of Liners for Conical Shaped Charges: Practicality and Performance," in *Proceedings of the Forty-Fifth Conference on Explosives and Blasting Technique, Jan. 27th – Jan. 30th 2019, International Society of Explosives Engineers*, Nashville, Tennessee, 2019.

[39] Accurate Energetic Systems, ""Linear Shaped Charge"," [Online]. Available: http://www.aesys.biz/wp-content/uploads/14-102_liner-shaped-charge.pdf.

[40] P. Mulligan, *LSC Bases,* January 17, 2019, Personal email.

[41] J. Plumridge, "What is Barrel Lens Distortion?," Lifewire, 13 January 2020. [Online]. Available: https://www.lifewire.com/what-is-barrel-lens-distortion-493725. [Accessed 25 October 2020].

[42] J. E. Fritz, "Separation Joint Technology," in *39th AIAA/ASME/SAE/ASEE Joint Propulsion Conference*, Huntsville, 2003.

VITA

Jason Ho was born in Edina, Minnesota. He attended grade school in Eden Prairie, Minnesota and graduated from Eden Prairie High School in June 2004. He received his Bachelor of Science degree in Chemistry from the University of Minnesota, Twin Cities in May 2016. He received his Master of Science degree in Explosives Engineering from Missouri University of Science and Technology in December 2020.